Evaluation of Network Expansion Decisions for Resilient Interdependent Critical Infrastructures with Different Topologies

Achara Tiong[a,1,*], Hector A. Vergara[a]

[a]*School of Mechanical, Industrial, and Manufacturing Engineering, Oregon State University, 204 Rogers Hall, Corvallis, OR 97331, USA*

Abstract

Resilient interdependent critical infrastructures (CIs) can better withstand cascading failures in disruptive events. This study proposes network expansion as a resilience improvement strategy for interdependent CIs and evaluates the influence of topology in interdependent network design for resilience optimization under disruption uncertainty. A resilience score consisting of network complexity and unmet demand metrics is introduced to quantify the resilience of expanded networks. Five synthetic interdependent network instances with random and hub-and-spoke (i.e., cluster) topologies are generated to represent CIs with heterogeneous node functions. Different network expansion opportunities are considered and critical node disruption scenarios are used to evaluate the impact of uncertain disruptions. We apply a two-stage stochastic multi-objective resilience optimization model to determine strategic investment decisions using the expected total cost and expected resilience score as competing objectives. Compromise solutions of expanded network designs are identified from Pareto optimal solutions and they are characterized according to their graph properties. The results show that expanded networks have improved resilience and the extent of improvement is affected by the network topology and type of disruption. Under critical node disruptions, a random network is more resilient than a hub-and-spoke structure due to its better connectivity. Characteristics of highly connected interdependent networks are high average node degree, high clustering coefficient, and low average shortest path length. Resilience improvement is more limited in expanded networks with a hub-and-spoke structure due to the negative impact of hub failures.

Keywords: Interdependent networks, Resilience, Network expansion, Two-stage stochastic programming, Multi-objective optimization, Network topology

Declarations of interest: None

*Corresponding author

Email addresses: acharationg@lifetime.oregonstate.edu (Achara Tiong), hector.vergara@oregonstate.edu (Hector A. Vergara)

1. Introduction

Critical infrastructures (CIs) such as electric power, natural gas, water supply, and telecommunication systems provide essential services to maintain the quality of life in modern society. CI networks are often interdependent having a bidirectional relationship such that the state of one CI influences that of the other [1, 2]. Basic types of interdependencies have been described as physical, cyber, geographic, logical, and social interactions [1, 3]. Due to these interdependencies, CIs are especially vulnerable to cascading failures across multiple systems when disruptions occur.

CI disruptions are caused by extreme events such as man-made failures, malevolent attacks, or natural disasters. In the U.S., the majority of CI disruptions are initiated by severe weather events [4]. There is ample evidence of large-scale interdependent CI failures from natural hazards over the past decade. The vulnerability of power-gas systems was evident during the 2021 Texas Blackout when power generation was curtailed by a disrupted gas supply during a historic snowstorm [5]. Earlier in 2012, power restoration in the aftermath of Hurricane Sandy was hampered by flooded roadways due to downed pumping stations [6]. Since gas distribution, transportation, and water supply systems rely on electrical power for their functionality, any disruption impact is exacerbated by the interdependencies between these networks. Resilient CIs are key to mitigating the losses of critical services and economic activities in disruptive events.

CI resilience refers to the ability of the infrastructures to absorb the initial shock of disruption, adapt to changing conditions, and timely restore basic functionalities following a disruption [7–11]. From the perspective of long-term CI resilience, network topology plays an important role in the assessment of structural vulnerability. Underlying structures of CIs have been characterized based on the network topological features observed in random, hub-and-spoke (cluster), grid, or hybrid graphs [12, 13]. These topologies affect the scale and propagation of cascading failures in interdependent CIs differently [14]. Resilience analysis that only considers one type of topology will have a limited interpretation. Considerations should be given to different network topologies that resemble real-world infrastructures.

Actions to enhance CI resilience are categorized as proactive or reactive decisions [15]. These decisions are evaluated according to the extent of improvements in the CI performance post-event. In this context, optimization models have been developed to support reactive or proactive decision making associated with disruptive events of interest [16]. Our study focuses on the proactive resilience improvement strategy of network expansion and determines recovery options for preparedness planning [17]. Considering interdependent CI networks with different topologies, we apply the mathematical formulation developed in our previous work [18] to analyze the topology effect on network expansion decisions. Stochastic disruptive events are incorporated into our model to account for uncertainty. Insights from this study can help decision-makers prioritize topology-based resilience investments over a strategic planning horizon.

The objective of our study is to assess the role of network topology in resilience as network expansion decisions are made for interdependent CIs under disruption uncertainty. To achieve this goal, we first consider interdependent network instances that are synthesized from a combination of commonly studied topologies.

Then, we apply the stochastic multi-objective optimization model for network expansion of interdependent CIs proposed in [18] to characterize the optimal expected solutions incorporating different scenarios. The main contributions of this study are to (a) present a methodology to generate interdependent networks with different topologies for computational experimentation, (b) introduce an approach to identify critical network components for disruption scenario generation, and (c) demonstrate the analysis of different topologies for resilient interdependent CIs through case studies of network instances that are representative of real-world applications.

This paper is organized as follows. Section 2 presents a review of existing literature pertaining to different types of interdependent networks and resilience optimization models. Section 3 describes the problem definition and reviews the model formulation for network expansion under uncertainty. The synthetic interdependent networks with different topologies and the disruption scenarios are shown in Section 4. Computational results and the characterization of solutions are presented in Section 5. Discussions and Lessons Learned are presented in Section 6 with conclusions and recommendations for future research summarized in Section 7.

2. Literature Review

CIs are usually studied as complex networks since they rarely function in isolation but rather interactively with other systems. The simplest form of interdependent CIs can be represented by two networks in which nodes in one network are connected by a bidirectional link to nodes in the other network [19]. Due to the heterogeneous roles of nodes, e.g., supply, transshipment, and demand nodes in each infrastructure, the functional relationships within CI networks are analogous to those observed in logistic networks with supply-demand links [20]. This enables CI performance and resilience measures to be analyzed using a network-based approach [21, 22].

For network-based models, CI network performance has been measured using topology-based and service-based methods [22, 23]. In a topology-based approach, the network topological characteristics are used to identify the structural vulnerability which plays a dominant role in long-term planning [24]. On the other hand, service-based performance metrics are required to accurately model cascading failures [25, 26] since they account for the functional relationships (e.g., flow characteristics) and the ability to satisfy customer demand [22, 27]. Common topology-based and service-based performance metrics are discussed in [22, 23, 27].

On a temporal basis, CI resilience has been assessed using frameworks that are based on static system survivability [28–30] vs. dynamic system recoverability [9, 31, 32]. *Static resilience* refers to the inherent system efficiency to withstand disturbances and survive impact without adaptive activities. Static resilience measures have been used to inform decisions in proactive strategies, e.g., retrofitting, fortification, and network expansion where decisions are taken before disturbances [33, 34]. In comparison, *Dynamic resilience* focuses on the speed of system recovery through time-dependent metrics that measure the losses of functionality over time. Dynamic resilience measures have been widely adopted for use in

reactive strategies, e.g., resource prioritization and restoration scheduling in which post-disruption responses are needed [35–38]. For comprehensive reviews of CI resilience assessment frameworks, we refer the reader to [9, 10, 39].

There is limited research that currently focuses on proactive resilience improvement decisions for interdependent CIs through network expansion. Conversely, a large body of literature focuses on developing mathematical models to optimize resilience for interdependent CIs via recovery and restoration [40–45]. In both proactive and reactive strategies, a common resilience measure used is the *unmet demand*, i.e., the inability to satisfy anticipated demand at demand nodes[46–48]. For problems related to proactive resilience strategies of network expansion as in [34, 49–51], the structural characteristics are often ignored. We address this gap by incorporating both network serviceability and structural properties as resilience metrics for network expansion. In addition to the *unmet demand*, we include the *network complexity*, i.e., the total number of nodes and links [52–54], as a structure-based metric in our study.

2.1. Interdependent Critical Infrastructure Networks

The characterization of real-world CI network topology has been extensively studied in an attempt to accurately model network vulnerability and cascading failures. For generic CIs, analysis of topology, spatial properties, and flow distribution are presented by [55, 56]. Various studies also focus on specific infrastructures such as power grids [57–60], transportation [48, 61], and water distribution [62]. Using a complex network theory approach, relationships between CI structures and network performance are established through graph characteristics. We first review graph models for individual infrastructures followed by the approach to build interdependency across networks.

Well-established graph models such as Erdős-Rényi random graphs [63], Watts-Strogatz small-world networks [64], and Barabási-Albert preferential attachment (scale-free) networks [65] have been used to analyze infrastructures such as transportation, communication, the internet, and power grid systems [61]. Random graphs generally have exponential degree distribution, small-world networks are highly clustered, and scale-free networks exhibit a power-law degree distribution [64, 66]. These network models allow graphs to be generated with controlled topologies and characterized through graph metrics such as the network size, degree distribution, clustering coefficient, and shortest path length [56]. As an example, one of the major electrical grids in the U.S., the Eastern Interconnection, consists of 49,597 nodes, 62,985 links, an average degree of 2.54, an average clustering coefficient of 0.071, and an average shortest path length of 35.8 [57]. Power grids have exponential degree distribution which is a common characteristic of a random graph [57]. A review of graph metrics used in power grid analysis can be found in [67].

Other related research has focused on optimizing the topology of the network so that it is able to withstand cascading failures and improve its robustness. For example, [68] and [69] apply this approach using memetic evolutionary algorithms to the design of wireless sensor networks for different network types including scale-free and random networks. [68] further explores the correlations between network properties and the robustness of the network against cascading failures.

While graph models provide a universal basis for topology generation, network connectivity is addressed on a case-by-case basis depending on applications. For practical reasons, network connectivities are established according to the flow direction of network commodities, i.e., material goods or services of the CIs. This is generally determined by the physical or operational functions of nodes and links in the network. For instance, water in the distribution system flows from the pump supply nodes to residential demand nodes, but not in the opposite direction [70]. In contrast, transmission power flow and smart grid flow can be bidirectional [71, 72]. Water and power are considered physical commodities of the infrastructure networks in this example.

From our literature review, network sizes for real-world interdependent network instances used in mathematical optimization problems are presented in Table 1. Due to the strong reliance on electricity, a large number of interdependent CI studies involve the power network. The graph representation of a power network captures the main electrical connectivity rather than actual physical connections thereby reducing the network instance size and the computational complexity of mathematical models.

Table 1: Real-world interdependent critical infrastructure network sizes in optimization problems

Interdependent Networks	Critical Infrastructure			Network 1		Network 2		Network 3		Reference
	Network 1	Network 2	Network 3	$\|N\|$	$\|A\|$	$\|N\|$	$\|A\|$	$\|N\|$	$\|A\|$	
Italian transmission grid and internet networks	Power	Communication		310	391	39	58			[73, 74]
Harris County, TX power-gas systems	Power	Gas		417	551	63	67			[75]
Shanghai power and electrified transportation networks	Power	Transportation		18	18	352	615			[76]
Galveston, TX power-transportation systems	Power	Transportation		62	70	16	44			[77]
US Northeast joint gas-power grid networks	Power	Gas		36	121	125	143			[78]
Belgian IEEE 14-bus power-gas systems	Power	Gas		14	80	22	24			[79]
Shelby County, TN power-water networks	Power	Water		60	76	49	71			[28, 42, 80–82]
Shelby County, TN power-water-gas networks	Power	Water	Gas	60	76	49	71	16	17	[27, 35, 50, 83, 84]

Note: $|N|$ = number of nodes and $|A|$ = number of links.

Instance generation algorithms for interdependent networks are proposed for common power-water systems in [37, 45, 85]. The limitation of these graph generation models is that they only consider undirected networks. Interdependent networks are not only coupled in a topological sense, but they also rely on the distribution of supply and demand nodes and the routing of flow [12, 13]. Assessing service-based performance in networks with heterogeneous node functions requires understanding the network connectivity and flow direction. Thus, networks that are generated as undirected graphs are not able to capture the interdependencies [28]. To our knowledge, there is no established graph model for generating connections in directed supply-demand networks with heterogeneous node functions. The challenge is to implement a directed graph generation approach that not only builds networks with characteristics of a certain topology but also creates link connectivity that complies with the flow direction

of the interdependent networks.

Finally, studies have shown that different network topologies are not equally tolerant to the same type of disruptions [56, 66]. Scale-free networks are resilient to random failures but more vulnerable to targeted attacks, especially on the hub nodes [86]. Alternatively, random graphs appear to be equally vulnerable to both random and targeted disruptions [55, 57]. Regardless of the topology, disruptive events contain certain levels of unpredictability thereby requiring resilience strategies to accommodate many possible disruption scenarios. We address this through a scenario-based stochastic programming approach which requires scenario generation and sampling within the representative scenario space.

2.2. Scenario Generation and Scenario Reduction

In most research studies, the evaluation of CI resilience requires generating disruption scenarios to represent situations of interest. However, scenarios that describe all uncertainty are rarely possible. While more uncertainties can be explained using a higher number of scenarios, it is computationally expensive. In this context, unrealistic scenarios are eliminated and scenarios that represent the possible realizations of the most likely situations are modeled [87]. Scenario generation strategies can be based on complete enumeration, sampling, optimization, strategy-specific, and situation-specific [21, 33, 88]. Since complete enumeration is unmanageable in large problems, a subset of scenarios is often determined using simulation, sampling techniques, or statistical analysis. An example of the optimization approach includes solving flow interdiction problems to determine the upper and lower bounds of disruption impact (best/worst case). On the other hand, situation-based disruptions involve manual selection [88].

Strategy-based disruptions fall under three categories: random, targeted, and spatial failures [89, 90]. In random disruptions such as component failures or human error, all network elements have an equal probability of being damaged. Targeted attacks involve critical component disruptions in which critical nodes or links are forced to fail to maximize damage as in the case of malevolent acts. In spatial disruptions, network components that are geographically co-located are affected which is often the case for natural disasters.

Scenario generation methods can be combined to create a representative sample. For example, Monte Carlo simulation is used in [33] to generate earthquake scenarios followed by network modeling and regression analysis to identify critical links of a road network in Salt Lake County, UT. In [91], disruption scenarios for transportation fuel infrastructure in Manhattan, NY incorporate different levels of flood hazards, fuel station availability, and fuel demand. In [92], scenarios of energy demand in distributed energy systems of Shanghai, China are generated from Monte Carlo simulation and reduced using the clustering method. A similar approach is found in [93] where scenarios are generated to capture the seasonal randomness of renewable energy demand in Norway using sampling, k-mean clustering, and distance-in-moments optimization methods. In power systems, sampling of interesting scenarios is used in [71] and scenario-reduction techniques that use forward- and backward-selection methods based on the distances between scenario pairs are described in [38, 94, 95]. For an empirical analysis of scenario generation methods in stochastic optimization, interested readers can consult [96].

3. Problem Definition

Interdependent CI systems consist of multiple individual CI networks that are heterogeneous in their topological structures and functional relationships between network elements. While most resilience optimization models place a strong emphasis on understanding functional relationships, the effects of the topology of individual networks and their expansion on resilience, specifically for interdependent systems, have not been well studied.

To address this challenge, we analyze the effect of network topologies on resilient interdependent CIs. This study presents a method to generate synthetic interdependent networks with different topologies and heterogeneous node functions. We incorporate different expansion opportunities for single vs. multiple networks. An approach to scenario planning is provided to capture disruption uncertainty.

With our network-based model, we apply the two-stage stochastic multi-objective resilience optimization model for interdependent network expansion presented in [18]. The goal is to optimize both the *expected total cost* and the *expected resilience* measured from network complexity and unmet demand metrics over a set of disruption scenarios. First-stage decisions involve determining the candidate nodes and links to add to the interdependent networks. Second-stage decisions determine the flow of commodities in the expanded networks, the unmet demand, and the unused supply at different nodes of the CI networks. These decisions must satisfy network operability rules related to the system capacity, minimum demand constraints, and physical interdependency. In the next section, we re-introduce the model formulation from our previous work in [18]. Multi-objective optimal solutions obtained with an exact solution approach are then characterized through graph metrics to evaluate the topology effect on resilience.

The multi-objective stochastic resilience optimization model from [18] was developed with the simplifying assumptions below.

- Each physical network operates interdependently on its intrinsic commodities and commodities originating from external networks.
- The movement of physical commodities between network nodes occurs through directed links which are restricted to one commodity type per link.
- The node status is discrete, i.e., the node is either fully functional or non-functional.
- Demand nodes are only functional if a specific percentage of the anticipated demand is met.
- In all disruption scenarios, candidate nodes and links are assumed to be non-disrupted.
- The fixed cost of candidate nodes and links including the unit costs of commodity flow are assumed to be scenario-independent.
- The resilience measure is calculated for the expanded network post-disruption at a steady state.

The interdependent relationships in our study are modeled by linking the demand node status to its ability to meet demand. Effectively, a non-disrupted demand node is functional if the satisfied demand exceeds the minimum demand threshold and is non-functional otherwise.

3.1. Stochastic Model for the Resilient Interdependent Network Expansion Problem

Table 2 shows the notation for sets and parameters used in the mathematical formulation. Table 3 shows the notation for the decision variables.

Table 2: Sets and parameters of the stochastic resilience optimization model for interdependent networks.

Sets	
Ω	Set of possible disruption scenarios ω
K	Set of interdependent infrastructure networks k
R	Set of commodities r from a single network in interdependent infrastructure networks
R^k	Set of commodities r from a single network in interdependent infrastructure network $k \in K,\ R^k \subseteq R$
$\bar{R}^k$	Set of commodities r not originating from interdependent infrastructure network $k \in K,\ \bar{R}^k \subseteq R^k$
N^k	Set of nodes i in network $k \in K$
N_s^{rk}	Set of supply nodes for commodity $r \in R^k$ in network $k \in K,\ N_s^{rk} \subseteq N^k$
N_t^{rk}	Set of demand nodes for commodity $r \in R^k$ in network $k \in K,\ N_t^{rk} \subseteq N^k$
N_o^{rk}	Set of transshipment nodes for commodity $r \in R^k$ in network $k \in K,\ N_o^{rk} \subseteq N^k$
N_c^k	Set of candidate nodes (facilities to open) in network $k \in K,\ N_c^k \subseteq N^k$
A^k	Set of links (i,j) between nodes $i,j \in N^k : i \neq j$ in network $k \in K$
$\bar{A}^{k,\omega}$	Set of disrupted links (i,j) between nodes $i,j \in N^k : i \neq j$ in network $k \in K, \bar{A}^{k,\omega} \subseteq A^k$, for a scenario $\omega \in \Omega$
A_c^k	Set of candidate links (i,j) between nodes $i,j \in N^k : i \neq j$ in network $k \in K, A_c^k \subseteq A^k$
A^{kl}	Set of interdependent links (i,j) between nodes $i \in N^k$ in network $k \in K$ and $j \in N^l$ in network $l \in K :\ l \neq k$
$\bar{A}^{kl,\omega}$	Set of disrupted interdependent links (i,j) between nodes $i \in N^k$ in network $k \in K$ and $j \in N^l$ in network $l \in K :\ l \neq k, \bar{A}^{kl,\omega} \subseteq A^{kl}$, for a scenario $\omega \in \Omega$
A_c^{kl}	Set of candidate interdependent links (i,j) between nodes $i \in N^k$ in network $k \in K$ and $j \in N^l$ in network $l \in K : l \neq k, A_c^{kl} \subseteq A^{kl}$
Parameters	
p_ω	Occurrence probability of disruption scenario $\omega \in \Omega$
B	Budget limitation for the network expansion cost
F_i^k	Fixed cost of establishing node $i \in N_c^k$ in network $k \in K$
f_{ij}^k	Fixed cost of establishing link $(i,j) \in A_c^k$ in network $k \in K$
f_{ij}^{kl}	Fixed cost of establishing interdependent link $(i,j) \in A_c^{kl}$ between networks $k \in K$ and $l \in K : l \neq k$
c_{ij}^{rk}	Unit cost of flow on link $(i,j) \in A^k$ for commodity $r \in R^k$ in network $k \in K$
c_{ij}^{rkl}	Unit cost of flow on interdependent link $(i,j) \in A^{kl}$ for commodity $r \in R^k$ in networks $k \in K$ and $l \in K : l \neq k$
$s_i^{rk,\omega}$	Supply at node $i \in N^k$ of commodity $r \in R^k$ for network $k \in K$ under scenario $\omega \in \Omega$
$d_i^{rk,\omega}$	Demand at node $i \in N^k$ of commodity $r \in R^k$ for network $k \in K$ under scenario $\omega \in \Omega$
α^r	Minimum percentage of total demand for commodity $r \in R$ to be satisfied
β_i^{rk}	Minimum percentage of demand for commodity $r \in R^k$ to be satisfied at demand node $i \in N_t^{rk}$ in network $k \in K$
γ_i^{rk}	Minimum percentage of demand for commodity $r \in \bar{R}^k$ to be satisfied at demand node $i \in N_t^{rk}$ in network $k \in K$
$q_{ij}^{rk,\omega}$	Flow capacity in scenario $\omega \in \Omega$ for link $(i,j) \in A^k$ for commodity $r \in R^k$ in network $k \in K$
$q_{ij}^{rkl,\omega}$	Flow capacity in scenario $\omega \in \Omega$ for interdependent link $(i,j) \in A^{kl}$ for commodity $r \in R^k$ in network $k \in K$ and $l \in K : l \neq k$
C_{nco}	Normalization constant for the node complexity metric
C_{lco}	Normalization constant for the link complexity metric
C_{ud}	Normalization constant for the unmet demand metric
w_{co}	Importance weight of network complexity metric in the resilience objective function

Table 2 (Continued): Sets and parameters of the stochastic resilience optimization model.

w_{nco}	Importance weight of the node complexity for the network complexity metric
w_{lco}	Importance weight of the link complexity for the network complexity metric
w_{ud}	Importance weight of unmet demand metric in the resilience objective function

Table 3: Decision variables of the interdependent network resilience optimization problem.

First Stage Decision Variables	
$\mathbf{y}_i^k$	1 if node $i \in N^k$ in network $k \in K$ is used and 0 otherwise
$\mathbf{z}_{ij}^k$	1 if link $(i,j) \in A^k$ in network $k \in K$ is used and 0 otherwise
$\mathbf{z}_{ij}^{kl}$	1 if interdependent link $(i,j) \in A^{kl}$ in networks $k \in K$ and $l \in K : l \neq k$ is used and 0 otherwise
Second Stage Decision Variables	
$\mathbf{x}_{ij}^{rk,\omega}$	Flow on link $(i,j) \in A^k$ of commodity $r \in R^k$ in network $k \in K$ under scenario $\omega \in \Omega$
$\mathbf{x}_{ij}^{rkl,\omega}$	Flow on interdependent link $(i,j) \in A^{kl}$ of commodity $r \in R^k$ in networks $k \in K$ and $l \in K : l \neq k$ under scenario $\omega \in \Omega$
$\mathbf{u}_i^{rk,\omega}$	Unused supply at node $i \in N_s^k$ for commodity $r \in R^k$ in network $k \in K$ under scenario $\omega \in \Omega$
$\mathbf{v}_i^{rk,\omega}$	Unmet demand at node $i \in N_t^k$ for commodity $r \in R^k$ in network $k \in K$ under scenario $\omega \in \Omega$

The stochastic model optimizes two competing objectives: (i) the *expected total cost* of network expansion and (ii) the *expected resilience* of the expanded networks. The expected total cost objective is considered the primary one due to the significance of the investment required. The expected objective function values are minimized over a set of disruption scenarios $\{\omega_1, \cdots, \omega_n\} \in \Omega$ with known probabilities $\{p_{\omega_1}, \cdots, p_{\omega_n}\}$ such that $\sum_{\omega \in \Omega} p_\omega = 1$.

3.2. Expected Total Cost Objective

The expected total cost objective as shown in (1) minimizes the *fixed cost* of adding candidate nodes and links in the first stage and the expected value of the *variable costs* of flow allocation post-disruption, $\mathcal{Q}(\mathbf{y}, \mathbf{z}, \boldsymbol{\omega})$, in the second stage according to (2).

$$\underset{\mathbf{y},\mathbf{z}}{\text{Min}}\ \mathbf{Z}_1 = \sum_{k \in K} \left(\sum_{i \in N_c^k} F_i^k \mathbf{y}_i^k + \sum_{(i,j) \in A_c^k} f_{ij}^k \mathbf{z}_{ij}^k + \sum_{l \in K : l \neq k} \sum_{(i,j) \in A_c^{kl}} f_{ij}^{kl} \mathbf{z}_{ij}^{kl} \right) + \mathbb{E}\{\mathcal{Q}(\mathbf{y}, \mathbf{z}, \boldsymbol{\omega})\} \tag{1}$$

$$\mathcal{Q}(\mathbf{y}, \mathbf{z}, \boldsymbol{\omega}) = \underset{\mathbf{x},\mathbf{u},\mathbf{v}}{\text{Min}} \sum_{k \in K} \sum_{r \in R^k} \left(\sum_{(i,j) \in A^k} c_{ij}^{rk} \mathbf{x}_{ij}^{rk,\omega} + \sum_{l \in K : l \neq k} \sum_{(i,j) \in A^{kl}} c_{ij}^{rkl} \mathbf{x}_{ij}^{rkl,\omega} \right) \tag{2}$$

3.3. Expected Resilience Score Objective

The resilience score consists of the *network complexity* and *unmet demand* metrics which form the expected resilience objective function as shown in (3). As a structure-based metric, *network complexity* is determined from the total number of nodes and links. It is evaluated in the first stage with only candidate components considered to account for the incremental complexity. The *unmet demand*, $\mathcal{W}(\mathbf{y}, \mathbf{z}, \boldsymbol{\omega})$, is a service-based metric determined from the difference between the anticipated and the satisfied demands

from all non-disrupted demand nodes. The unmet demand in (4) depends on a scenario realization and its expected value is evaluated in the second stage. Both metrics are normalized and weighted. A network with a lower expected resilience score is considered more resilient to disruptions due to lower network complexity and lower unmet demand. Also, we can determine the network *service level*, i.e., the percentage of anticipated demand that is actually met, through the total unmet demand.

$$\underset{\mathbf{y},\mathbf{z}}{\text{Min}}\ \mathbf{Z}_2 = w_{co}\left(\sum_{k\in K}\left(\frac{w_{nco}}{C_{nco}}\sum_{i\in N_c^k}\mathbf{y}_i^k + \frac{w_{lco}}{C_{lco}}\left(\sum_{(i,j)\in A_c^k}\mathbf{z}_{ij}^k + \sum_{l\in K:l\neq k}\sum_{(i,j)\in A_c^{kl}}\mathbf{z}_{ij}^{kl}\right)\right)\right) + \tfrac{w_{ud}}{C_{ud}}\mathbb{E}\{\mathcal{W}(\mathbf{y},\mathbf{z},\boldsymbol{\omega})\} \tag{3}$$

$$\mathcal{W}(\mathbf{y},\mathbf{z},\boldsymbol{\omega}) = \underset{\mathbf{x},\mathbf{u},\mathbf{v}}{\text{Min}}\ \sum_{k\in K}\sum_{r\in R^k}\sum_{i\in N_t^k}\mathbf{v}_i^{rk,\omega} \tag{4}$$

3.4. Constraints

The constraints associated with the first-stage decisions are defined in (5)–(7). The second-stage constraints are presented in (8)–(20).

$$\mathbf{z}_{ij}^k \le \mathbf{y}_i^k \quad \forall (i,j)\in A^k,\ k\in K \tag{5}$$

$$\mathbf{z}_{ij}^{kl} \le \mathbf{y}_i^k \quad \forall (i,j)\in A^{kl},\ k\in K,\ l\in K: l\neq k \tag{6}$$

$$\sum_{k\in K}\left(\sum_{i\in N_c^k}F_i^k\mathbf{y}_i^k + \sum_{(i,j)\in A_c^k}f_{ij}^k\mathbf{z}_{ij}^k + \sum_{l\in K:l\neq k}\sum_{(i,j)\in A_c^{kl}}f_{ij}^{kl}\mathbf{z}_{ij}^{kl}\right) \le B \tag{7}$$

$$\sum_{(i,j)\in A^k}\mathbf{x}_{ij}^{rk,\omega} + \sum_{l\in K:l\neq k}\sum_{(i,j)\in A^{kl}}\mathbf{x}_{ij}^{rkl,\omega} - \sum_{(j,i)\in A^k}\mathbf{x}_{ji}^{rk,\omega} - \sum_{l\in K:l\neq k}\sum_{(j,i)\in A^{kl}}\mathbf{x}_{ji}^{rkl,\omega} = \begin{cases} s_i^{rk,\omega} - \mathbf{u}_i^{rk,\omega} & \forall i\in N_s^{rk},\ r\in R^k,\ k\in K,\ \omega\in\Omega \\ 0 & \forall i\in N_o^{rk},\ r\in R^k,\ k\in K,\ \omega\in\Omega \\ -d_i^{rk,\omega} + \mathbf{v}_i^{rk,\omega} & \forall i\in N_t^{rk},\ r\in R^k,\ k\in K,\ \omega\in\Omega \end{cases} \tag{8}$$

$$\mathbf{x}_{ij}^{rk,\omega} \le q_{ij}^{rk}\mathbf{z}_{ij}^k \quad \forall (i,j)\in A^k,\ r\in R^k,\ k\in K,\ \omega\in\Omega \tag{9}$$

$$\mathbf{x}_{ij}^{rkl,\omega} \le q_{ij}^{rkl}\mathbf{z}_{ij}^{kl} \quad \forall (i,j)\in A^{kl},\ r\in R^k,\ k\in K,\ l\in K: l\neq k,\ \omega\in\Omega \tag{10}$$

$$\sum_{k\in K}\sum_{i\in N_t^{rk}}\mathbf{v}_i^{rk,\omega} \le (1-\alpha^r)\sum_{k\in K}\sum_{i\in N_t^{rk}}d_i^{rk,\omega} \quad \forall r\in R,\ \omega\in\Omega \tag{11}$$

$$\mathbf{v}_i^{rk,\omega} \le d_i^{rk,\omega}\left(1-\mathbf{y}_i^k\right) + \left(1-\beta_i^{rk}\right)d_i^{rk,\omega}\mathbf{y}_i^k \quad \forall i\in N_t^{rk},\ r\in R^k\setminus\bar{R}^k,\ k\in K,\ \omega\in\Omega \tag{12}$$

$$\mathbf{v}_i^{rk,\omega} \le d_i^{rk,\omega}\left(1-\mathbf{y}_i^k\right) + \left(1-\gamma_i^{rk}\right)d_i^{rk,\omega}\mathbf{y}_i^k \quad \forall i\in N_t^{rk},\ r\in \bar{R}^k,\ k\in K,\ \omega\in\Omega \tag{13}$$

$$\mathbf{y}_i^k \in \{0,1\} \quad \forall i\in N^k,\ k\in K \tag{14}$$

$$\mathbf{z}_{ij}^k \in \{0,1\} \quad \forall (i,j)\in A^k,\ k\in K \tag{15}$$

$$\mathbf{z}_{ij}^{kl} \in \{0,1\} \quad \forall (i,j)\in A^{kl},\ k\in K,\ l\in K: l\neq k \tag{16}$$

$$\mathbf{x}_{ij}^{rk,\omega} \ge 0 \quad \forall (i,j)\in A^k,\ r\in R^k,\ k\in K,\omega\in\Omega \tag{17}$$

$$\mathbf{x}_{ij}^{rkl,\omega} \ge 0 \quad \forall (i,j)\in A^k,\ r\in R^k,\ k\in K,\ l\in K: l\neq k,\omega\in\Omega \tag{18}$$

$$\mathbf{u}_i^{rk,\omega} \geq 0 \quad \forall i \in N_s^{rk},\ r \in R^k,\ k \in K, \omega \in \Omega \tag{19}$$

$$\mathbf{v}_i^{rk,\omega} \geq 0 \quad \forall i \in N_t^{rk},\ r \in R^k,\ k \in K, \omega \in \Omega \tag{20}$$

Constraints (5) and (6) guarantee that the links may not be operational unless the origin nodes are also operational. Constraint (7) limits the budget of network expansion. Constraints (8) represent the commodity flow balance for the supply, transshipment, and demand nodes. Constraints (9) and (10) ensure that the commodity flow does not exceed the maximum capacity of the links. Constraints (11) ensure that a specific percentage of the total demand for commodity r must be met. The relationship between the unmet demand and the status of demand nodes is established in (12) and (13). These constraints enforce the minimum demand of commodities that must be met at the demand node for the node to be functional. Constraints (13) represent the physical interdependency between networks since the supply nodes of one network behave as demand nodes for the interdependent commodity. The constraints from (14) to (20) are the variable type constraints.

The two-stage stochastic multi-objective resilience optimization model for network expansion of CIs can be summarized as:

$$\text{Minimize } \mathbf{Z}_1 \ (1)$$

$$\text{Minimize } \mathbf{Z}_2 \ (3)$$

$$\text{Subject to} : (5) - (20)$$

This formulation is solved using an exact approach given the manageable size of the problem instances in this study. Using the multi-objective approach by [97], the stochastic MIP formulation is transformed into an equivalent deterministic problem through the two-stage stochastic program. Then, the deterministic multi-objective problem is solved using the augmented ϵ-constraint method to generate the Pareto efficient set of exact solutions [98].

4. Computational Experiments: Synthetic Interdependent Networks with Different Topologies

In this study, we consider random and hub-and-spoke topologies since their structures can be found in various physical systems [61, 66]. The random topology has been extensively studied in power grid vulnerability modeling since the physical structure is neither scale-free nor small-world and the degree distribution is exponential [12, 58]. Alternatively, a hub-and-spoke configuration contains scale-free characteristics, i.e., the spoke nodes are *preferentially attached* to the hub nodes that already have a high number of links thereby forming clusters. Examples of scale-free structures are air transportation, information (WWW), and communication networks. Graph metrics, e.g., the average node degree, average clustering coefficient, average shortest path length, and network diameter, are extensively used to characterize topologies. For instance, scale-free networks have low average clustering coefficients while

small-world networks have small network diameters and shortest path lengths. The definitions of graph metrics used in this study are shown in Table 4

The interdependent CI networks modeled in our study consist of two single networks that are connected by interdependent links. We refer to the two single networks within an interdependent network as A and B. To evaluate the topology effect, we consider two interdependent networks where A and B have (i) the same topology and (ii) two different topologies. Network A is a random network that is used in all instances. For network B, we consider random and hub-and-spoke topologies. In all instances, network B is smaller than network A to analyze the heterogeneity in network sizes.

Table 4: Network graph metrics for complex networks.

Graph Metric	Expression	Description
Average degree	$\langle \mathsf{k} \rangle = \frac{1}{\lvert N \rvert} \sum_{i \in N} \mathsf{k}_i$ where $\mathsf{k}_i = \mathsf{k}_i^{in} + \mathsf{k}_i^{out} = \sum_{j \in N} \mathsf{a}_{ij} + \sum_{j \in N} \mathsf{a}_{ji}$ (Directed graph)	Average number of links incident on a node in a graph. k_i = a degree of node i
Average clustering coefficient	$\langle \mathsf{c} \rangle = \frac{1}{\lvert N \rvert} \sum_{i \in N} \mathsf{c}_i$ where $\mathsf{c}_i = \frac{2\mathsf{T}_i}{\mathsf{k}_i(\mathsf{k}_i - 1)}$	Average of the fraction of possible triangles through a node in an undirected, unweighted graph [64]. The clustering coefficient measures how tightly connected a node is to its neighborhood.
Average shortest path length	$\mathsf{L} = \frac{1}{\lvert N \rvert (\lvert N \rvert - 1)} \sum_{\substack{i,j \in N \\ (i \neq j)}} \mathsf{d}_{ij}$	Average number of links in the shortest path between a pair of nodes [57]. It measures the efficiency of information transport on a network. For a weighted graph, d_{ij} is replaced by the link's weight.
Network diameter	$\mathsf{d}_{max} = \max_{i,j}(\mathsf{d}_{ij})$	Maximum distance (number of links in the longest path) between all pairs of nodes [57].

Note: a_{ij} = element of the graph's adjacency matrix A corresponding to a link between nodes i and j. $|N|$ = number of nodes. T_i = Number of triangles through node i. d_{ij} = Length of the shortest path (geodesic path) between all pairs of nodes $i, j \in N, i \neq j$ and $\mathsf{d}_{ij} = 0$ if j is not reachable from i.

4.1. Instance Generation

We first synthesize three individual networks: Random A, Random B, and Hub-and-spoke B. The networks are generated to include all existing and candidate nodes which are positioned randomly within a unit circle. The network structure is controlled through the connections between nodes. We generate the directed graphs to ensure connectivities, i.e., there must be a path of commodity flow between the supply and demand nodes so that demand can be satisfied. The distance of a link between two nodes is based on Euclidean distance.

For Random A and Random B, the heterogeneous node types, i.e., supply, demand, and transshipment, are randomly assigned. We allocate a portion of each node type as candidates for network expansion. Then, we add directed links to connect the origin-destination node pairs with the following rules: there is at least one outflow from supply nodes, transshipment nodes must have at least one outflow and one inflow, and demand nodes must have at least one inflow. The connections are prioritized based on the shortest Euclidean distance between nodes. Links adjacent to the candidate node are also made candidate links.

For Hub-and-spoke B, the supply nodes are considered the *hub* of each cluster, and the non-supply nodes are the *spoke* nodes. We create the hub-and-spoke connectivity using the k-medoid clustering algorithm [99] to identify the location of k supply nodes as the medoids and the non-supply nodes as members of each

cluster. Directed links are added to form the hub-and-spoke connections. Then, the non-supply nodes are randomly assigned as demand and transshipment nodes as per the network specification. Inflow and outflow links are added to the transshipment nodes according to the previously-stated rules to ensure connectivity. We allow for multiple allocations, i.e., demand nodes can receive flow from more than one supply node. To ensure that no clusters are isolated from the rest of the network, we randomly add links between supply nodes. A portion of supply nodes is assigned as candidate nodes thereby making their associated clusters a part of candidate components for expansion.

The network specifications for Random A, Random B, and Hub-and-spoke B are provided in Table 5. We assume that each network is associated with a single commodity, i.e., network A and B transport commodities a and b, respectively. The number of nodes and the proportion of supply, transshipment, and demand nodes are chosen such that they resemble those commonly found in the CI literature involving mathematical optimization problems [50, 73–75, 79].

Table 5: Node and link types of the synthetic networks.

Graph Topology Network	Random A	Random B	Hub & spoke B
Commodity	a	b	b
Existing Network Components			
No. of Nodes	354	56	56
Supply	55	9	9
Transshipment	117	18	4
Demand	182	29	43
No. of Links	536	88	66
Candidate Network Components			
No. of Nodes	47	17	25
Supply	6	4	4
Transshipment	6	0	4
Demand	22	7	17
No. of Links	131	32	35

The synthetic networks Random A, Random B, and Hub-and-spoke B are shown in Figure 1. We remove the candidate components from the graphs to illustrate the baseline (existing) network before expansion. The comparison of network characteristics between the synthetic networks and the reference random graphs of similar size are shown in Table 6. These reference graphs are modeled using the Erdős-Rényi (ER) random, Watts-Strogatz (WS) small-world, and Barabási-Albert (BA) preferential attachment mechanisms with the same number of nodes and a similar number of links.

From Table 6, we observe that the network Random A consists of a similar average node degree as the ER random graph model. The longer average shortest path length (L) indicates a characteristic of the preferential attachment model since ER graphs generally have smaller L. The larger average clustering coefficient for Random A also shows a small-world characteristic. For Random B, the average node degree and network diameter resemble those of the ER model; however, we observe high clustering. The Hub-and-

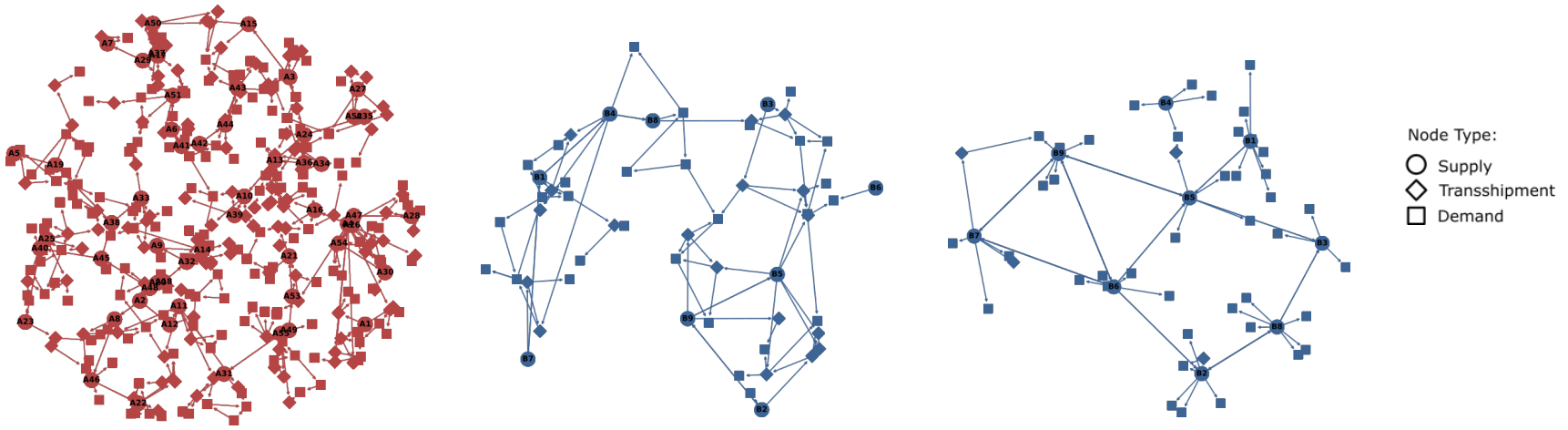

(a) Random A (b) Random B (c) Hub-and-spoke B

Figure 1: Synthetic infrastructure networks A and B without candidate nodes. The supply, transshipment, and demand nodes are indicated by the circle, diamond, and square nodes, respectively.

Table 6: Comparison of graph properties of the infrastructure networks A and B without candidate nodes.

Number of Nodes	354	354	354	354	56	56	56	56	56
Graph Type	Random A	Random (ER)	Preferential Attachment (BA)	Small-World (WS)	Random B	Hub&Spoke B	Random (ER)	Preferential Attachment (BA)	Small-World (WS)
Number of Links	538	538	353	708	88	66	87	108	112
Avg. Node Degree	3.03	2.93	1.99	3.29	3.14	2.36	3.00	2.98	3.40
Max. Node Degree	13	8	26	8	7	12	7	16	6
Network diameter*	10	29	14	10	8	6	11	5	6
Avg. Clustering Coefficient*	0.1518	0.0085	0.0010	0.2558	0.2203	0.0781	0.0753	0.1804	0.2593
Avg. Shortest Path Length*	9.98	5.24	6.33	5.56	5.00	3.73	3.37	2.78	3.43

* Undirected and unweighted graph

spoke B network shows a high maximum node degree that is similar to the scale-free (BA) model. These synthetic networks are further characterized through the cumulative degree distribution in Figure 2. We observe that the Random A network exhibits the characteristics of the random ER model with a preferential growth in Figure 2a. For the smaller networks in Figure 2b, Random B approximates the purely random ER model reasonably well. The preferential attachment structure is more prominent in Hub-and-spoke B due to the presence of the supply nodes acting as hub nodes with a higher degree than most other nodes.

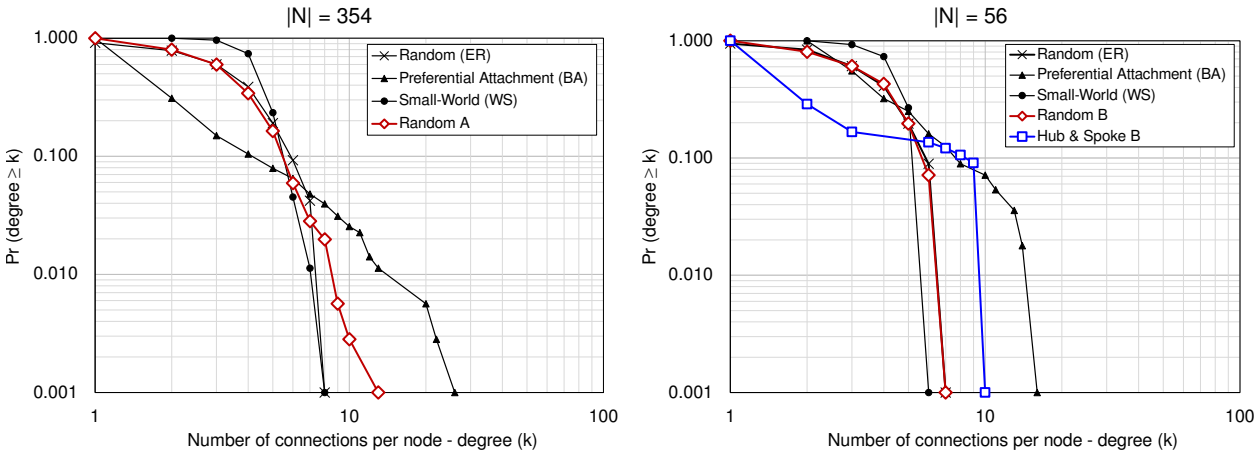

(a) 354-node networks (b) 56-node networks

Figure 2: Cumulative degree distribution of synthetic network graphs

We confirm the preferential attachment observations with the node degree distribution by node type for Random A, Random B, and Hub-and-spoke B in Figure 3. It is observed that the long-tailed degree distribution in the Random A network is largely attributed to the supply nodes. This is illustrated more clearly in the degree distribution for Hub-and-spoke B given the high degree of supply nodes. In contrast, the node degree in Random B appears to be more randomly distributed across the three node types.

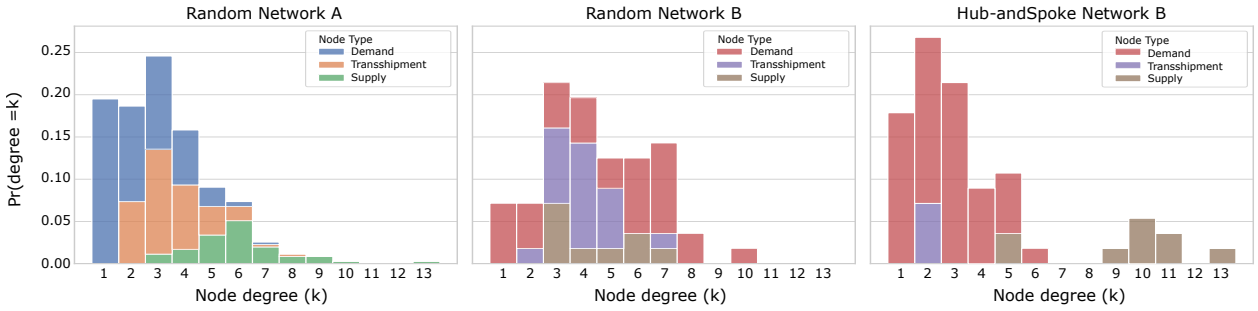

Figure 3: Node degree distribution by node type for Random A, Random B, and Hub-and-spoke B networks.

4.2. Interdependent Networks

To establish the interdependency between the two networks, we add bidirectional links between networks A and B. The interdependency is assumed to be a physical relationship, i.e., the state of one network depends on receiving a physical flow of commodities from the other network. For simplicity, we refer to

the commodity that does not originate from its network as an *external* commodity, e.g., b is an external commodity to network A, and vice versa. We assume that a fraction of supply nodes in each network requires an external commodity that can be drawn from the other network's demand nodes. Thus, we add directed links across network boundaries by prioritizing the connections that are among the lowest distances. While the properties of a and b are abstract in nature, they are required to be representative of physical or logical flows in directed links of interdependent networks A and B according to our modeling assumptions.

In this study, we consider a total of five problem instances based on combinations of different network structures for interdependent networks and expansion opportunities. The instances have either a structure of Random A – Random B (RR) or Random A – Hub-and-spoke B (RH) for the two interdependent networks. Additionally, three expansion opportunities are considered where candidate nodes belong to network A only, network B only, and to both networks A and B (AB). We denote the five interdependent network instances with the following case names: RR_A, RR_{AB}, RH_A, RH_B, and RH_{AB}. The first two characters indicate the network structure of A and B and the subscript represents the expansion options, e.g., case RH_{AB} refers to the Random A – Hub-and-spoke B interdependent networks with both A and B candidates for expansion. The graph properties for the five interdependent network instances are summarized in Table 8. For illustration purposes, the instance for RH_{AB} is shown in Figure 4.

4.3. Model Data Generation

The values for the model parameters used in this study are shown in Table 7. The candidate node costs are assigned according to the node types with supply nodes being the most expensive assets. The cost to open a candidate link is proportional to its length. We specify an unrestricted budget value such that all candidate nodes and links can be opened. For the expected resilience objective, the component weights w_{co} and w_{ud} for the network complexity and unmet demand metrics are set to prioritize the service-based network performance [17]. The total service levels of at least 40% for both networks A and B are specified. Each non-disrupted demand node also requires at least 40% of the anticipated demand to be met. The minimum percentage of external commodity demand is set at 60% for appropriate demand nodes in both networks.

4.4. Disruption Scenario Generation and Scenario Reduction

Disruption uncertainty is introduced through a scenario-based optimization approach. Scenarios are generated to represent critical node disruptions in the Random A which is the larger network. We apply node disruptions based on a previous study by [28] which removes strategic nodes to impair network connectivity. In a node disruption, both the nodes and their adjacent links are simultaneously removed which creates a greater disruption impact than the link disruption alone.

We define a critical node as the node that produces the most network damage if disrupted, and the level of damage is measured through the reduction in maximum flow according to the framework by [21]. The procedure to generate critical node disruption scenarios is illustrated in Figure 5. First, we identify

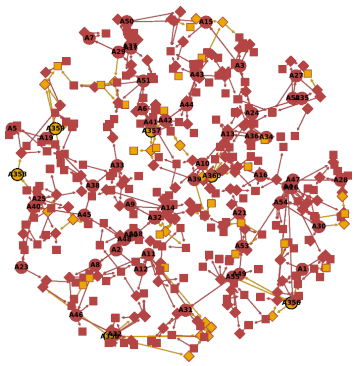

(a) Random A with candidate components

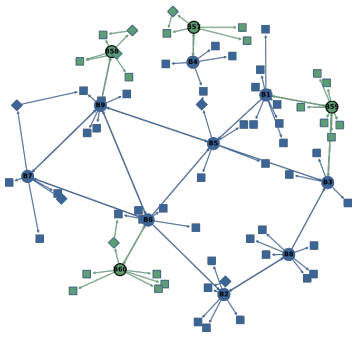

(b) Hub-and-spoke B with candidate components

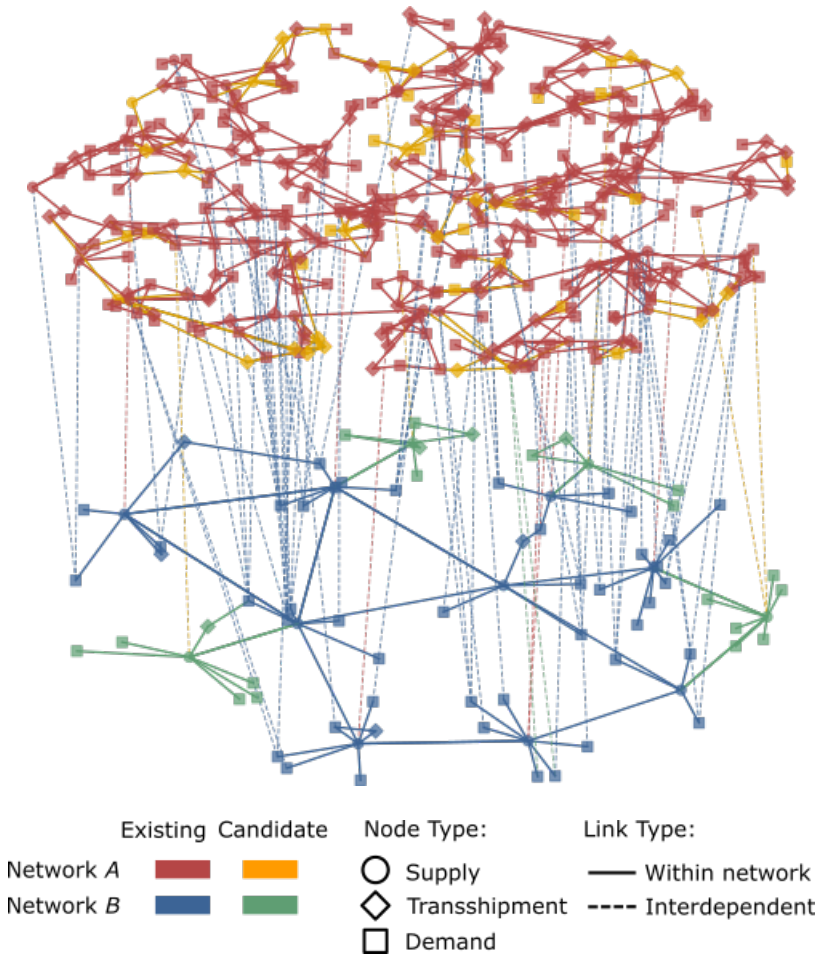

(c) RH_{AB}: Random A – Hub-and-spoke B with A and B candidate components

Figure 4: Synthetic Random A – Hub-and-spoke B interdependent networks with A and B expansion.

Table 7: Problem parameters.

Model Parameter	Value
w_{co}	0.15
w_{nco}, w_{lco}	0.50
w_{ud}	0.85
α^r, β_i^{rk}	10%
γ_i^{rk}	40%

Network Parameter		Value
Fixed cost	Candidate A node	Supply node: $\mathcal{U}$ ~(170, 250), Demand node: $\mathcal{U}$ ~(35, 55), Transshipment node: $\mathcal{U}$ ~(40, 60)
	Candidate B node	Supply node: $\mathcal{U}$ ~(175, 215), Demand node: $\mathcal{U}$ ~(35, 55), Transshipment node: $\mathcal{U}$ ~(40, 60)
	Candidate link	$A-A$ and $B-B$: 15+70*length, $A-B$ and $B-A$: 2.5% premium
Budget		10,000
Unit flow cost	a and b	0.15
Supply & Demand	Candidate A supply node	Supply a: $\mathcal{U}$ ~(50, 100), Demand b (external): $\mathcal{U}$ ~(5, 10)
	Candidate A demand node	Demand a: $\mathcal{U}$ ~(4, 80)
	Candidate B supply node	Supply b: $\mathcal{U}$ ~(50, 100), Demand a (external): $\mathcal{U}$ ~(5, 10)
	Candidate B demand node	Demand b: $\mathcal{U}$ ~(5, 15)
Link capacity	$A-A$ and $A-B$	10.0
	$B-B$ and $B-A$	40.0

Table 8: Graph properties of the synthetic interdependent networks.

Instance	RR_A			RR_{AB}			RH_A			RH_B			RH_{AB}		
Graph Topology	Random	Random		Random	Random		Random	Hub&Spoke		Random	Hub&Spoke		Random	Hub&Spoke	
Network	A	B	Total	A	B	Total	A	B	Total	A	B	Total	A	B	Total
Expansion	Yes	No		Yes	Yes		Yes	No		No	Yes		Yes	Yes	
Existing Components															
No. of Nodes	354	56	410	354	56	410	354	56	410	354	56	410	354	56	410
No. of Links	544	155	699	544	155	699	543	133	676	543	133	676	543	133	676
Link $A-B$	8	-		8	-		7	-		7	-		7	-	
Link $B-A$	-	67		-	67		-	67		-	67		-	67	
Candidate Components															
No. of Nodes	47	0	47	47	17	64	47	0	47	0	25	25	47	25	72
No. of Links	131	3	134	136	35	171	131	2	133	5	35	40	136	37	173
Link $A-B$	0	-		5	-		0	-		5	-		5	-	
Link $B-A$	-	3		-	2		-	2		-	0		-	2	
Full Network (Existing and Candidate Components)															
No. of Nodes	401	56	457	401	73	474	401	56	457	354	81	435	401	81	482
Supply	61	9		61	13		61	9		55	13		61	13	
Transshipment	136	18		136	24		136	4		117	8		136	8	
Demand	204	29		204	36		204	43		182	60		204	60	
No. of Links	675	158	833	680	190	870	674	135	809	548	168	716	679	170	849
$A-A$	667	-		667	-		667	-		536	-		667	-	
$A-B$	8	-		13	-		7	-		12	-		12	-	
$B-B$	-	88		-	120		-	66		-	101		-	101	
$B-A$	-	70		-	70		-	69		-	67		-	69	
Avg. Node Degree	3.52	4.54	3.64	3.53	4.42	3.67	3.52	3.71	3.54	3.25	3.47	3.29	3.53	3.49	3.52
Max. Node Degree	13	10	13	13	10	13	13	13	13	13	15	15	13	15	15
Avg. Clustering Coefficient*			0.1615			0.1589			0.1527			0.1532			0.1532
* Undirected, unweighted graph															

the criticality of each node if disrupted individually by determining the overall network service levels after each of the 354 existing nodes in Random A are disrupted (Figure 5(a)). We observe that supply nodes, particularly those with a degree $(\mathsf{k}_i) \geq 6$, cause the most reduction in service level when damaged.

Subsequently, we demonstrate a scenario generation approach for multiple-node disruption starting with two critical nodes. Since the number of possible scenarios can be too large to be practical, we present a procedure to reduce the number of scenarios until a manageable sample size is reached. Initially, 33 supply nodes with $\mathsf{k}_i \geq 6$ are considered critical nodes. Then, all possible combination of the two-node disruption scenarios is performed ($\binom{33}{2} = 528$ samples, Figure 5(b)). We observe a greater range of impact to the maximum service level as one additional node is disrupted. Since the nodes with a high degree are more critical, the scenarios are further reduced by considering 15 supply nodes with $\mathsf{k}_i \geq 7$ ($\binom{15}{2} = 105$ samples, Figure 5(c)). We observe that the ten worst-case scenarios before and after scenario reduction only differ by two samples. For simplicity, we proceed with the ten worst-case samples of the two-node disruption scenarios considering the supply nodes with $\mathsf{k}_i \geq 7$. The ten scenario probabilities are equally distributed at 10%. To model parameter uncertainty in each disruption scenario, the capacities of the links adjacent to the disrupted node are set to zero to replicate the physical damage.

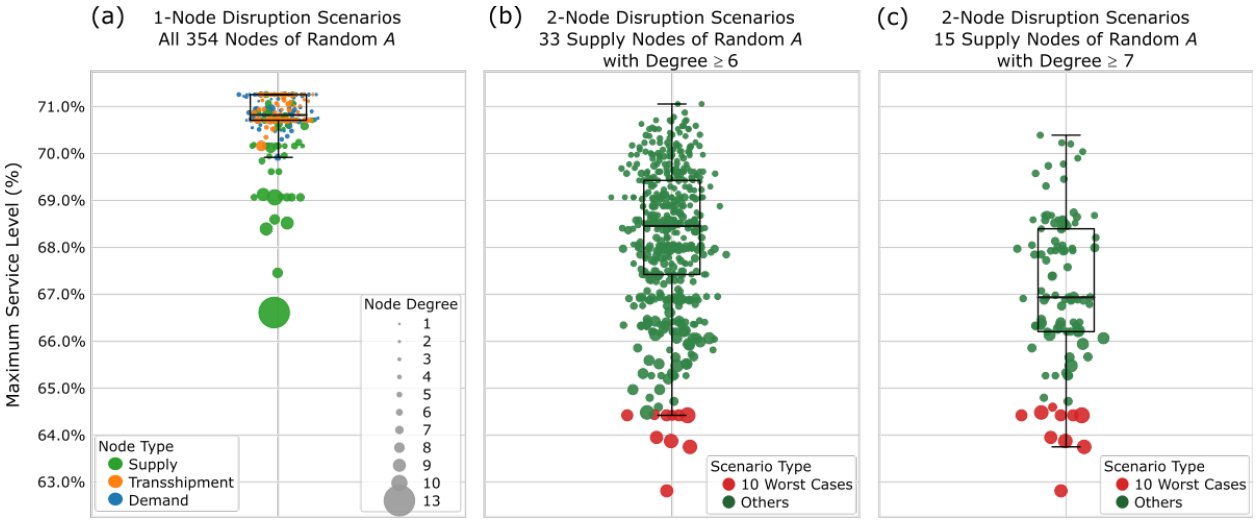

Figure 5: A scenario reduction approach for the critical node disruption.

5. Computational Results

We apply the multi-objective resilience optimization model for interdependent network expansion to the five problem instances described above. Each problem instance is solved for the same set of ten scenarios, i.e., two-critical node disruptions in Random A, with the same probability of occurrence. The two-stage stochastic programming problems are solved to optimality using a relative gap tolerance of 1E-4 as the termination criterion. A total of 20 multi-objective optimal solutions are obtained for each problem instance using the augmented ϵ-constraint method with ϵ = 1E-3. The computational experiments are performed

on an Intel® Xeon® E3-1231 CPU 3.40GHz with 16.0 GB RAM using CPLEX 12.9.0 on Python 3.7.6. All optimal solutions are obtained in approximately 9.1 seconds on average. The MIP problem and solver statistics are summarized in Table 9.

Table 9: Problem statistics for five test instances (number of objectives = 2).

Instance	RR_A	RR_{AB}	RH_A	RH_B	RH_{AB}
Total number of variables	13,170	13,744	13,046	11,951	13,961
Continuous	11,880	12,400	11,780	10,800	12,630
Binary	1,290	1,344	1,266	1,151	1,331
Total number of linear constraints	17,957	18,721	17,809	16,463	18,789
Inequality	12,867	13,421	12,719	11,573	13,409
Equality	5,090	5,300	5,090	4,890	5,380
Average solution time (seconds)	10.1	10.2	9.0	3.0	13.4
Minimum	3.4	3.6	6.9	1.9	6.7
Maximum	18.5	17.8	16.0	5.0	22.1

Figure 6 shows the Pareto optimal solutions for the five problem instances. The solutions corresponding to Random A – Random B and Random A – Hub-and-spoke B interdependent networks are shown in Figures 6a and 6b, respectively. Pareto optimal solutions are non-dominated solutions, i.e., each solution outperforms other solutions in at least one objective and are not worse than other solutions in all objectives. Recall that the expected total cost ($\mathbf{Z}_1$) and the expected resilience score ($\mathbf{Z}_2$) are two competing objectives. A lower $\mathbf{Z}_2$ indicates a more resilient network, and the Pareto solutions represent the trade-off of investing more in total cost to improve resilience. The objective function values, the total cost and resilience components, and the candidate nodes and links added are summarized in Table 10 to Table 14.

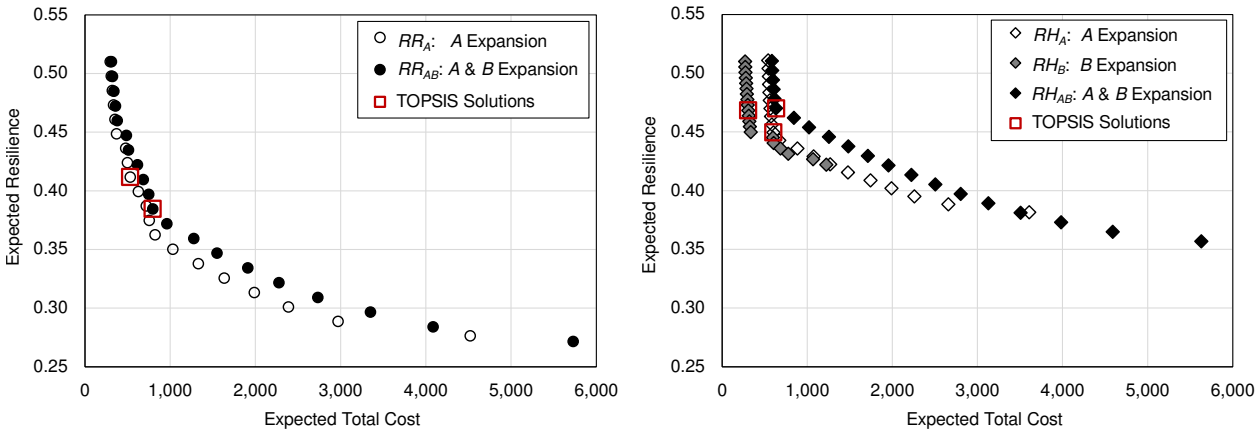

(a) Random A – Random B

(b) Random A – Hub & spoke B

Figure 6: Pareto optimal solutions.

From the Pareto fronts in Figure 6, the expected resilience score decreases with increasing total cost thereby illustrating the trade-off between the two objectives. We see that resilience can be improved (i.e., decreased resilience score) through network expansion. In fact, a significant reduction in the resilience score is achievable at lower-cost options. However, the improvement diminishes as the expected total cost increases.

For ease of analysis, we introduce a compromise solution that balances two optimal objectives from each Pareto front using a multi-criteria decision-making technique called Technique for Order of Preference by Similarity to an Ideal Solution (TOPSIS) [100]. Based on the concept that the best solution is closest to the positive ideal solution and furthest from the negative ideal solution, TOPSIS is a well-established comparative method that is extensively used given its simplicity and ease of implementation [101]. It allows us to select a single solution from the Pareto front for further evaluation without having to make any additional assumptions about decision-maker preferences between the two objectives. First, the two extreme points of the objective function values (i.e., Pareto front solutions) are identified as positive and negative ideal solutions. In our case, the lowest possible values of both objectives are considered the positive ideal solution. Then, the Euclidean distances between each Pareto solution relative to its ideal solutions are calculated and ranked. The Pareto solution with the shortest relative closeness to the positive ideal solution is identified as the *TOPSIS solution* which is considered as our suggested compromise solution. These solutions are indicated in Figure 6 with square markers.

We observe the largest variations in optimal solutions between the Random B (RR_A and RR_{AB}) and Hub-and-spoke B topologies (RH_A, RH_B, and RH_{AB}). Within the same topology, variations are less prominent among the expansion options, i.e., A, B, or both. Given the similar range of expected total costs, the RR instances have a greater opportunity to improve resilience through network expansion than the RH instances. For the highest expected total cost options, i.e., 5,728 for RR_{AB} and 5,630 for RH_{AB}, the resilience score of RR_{AB} (0.271) is approximately 25% lower than that of RH_{AB} (0.357). This result is also in line with the observation that hub-and-spoke networks are less resilient to critical node disruptions, especially on the supply (hub) nodes [86]. We see that interdependent networks containing a hub-and-spoke structure would require a higher cost for resilience improvement than those with a random topology. Additionally, the resilience gain would be more limited.

In terms of expansion opportunity, we first examine the post-disruption resilience of a single network expansion. As observed in Figure 6b between the RH_A and RH_B instances, expanding Random A alone can reduce (i.e., improve) the resilience score by up to 25%. In contrast, the maximum improvement in resilience from a Hub-and-spoke B expansion alone is more limited at 17%. In both RH_A and RH_B, we found that the unmet demand for commodity a contributes to greater than 67% of the total unmet demand in all solutions. Since Random A has a larger network size ($|N_A| > 6|N_B|$), the resilience score is influenced by the ability to meet demand in the larger network.

When comparing the expansion opportunities between A alone vs. both A and B, the resilience improvement from a two-network expansion appears marginal. Although adding more candidate components of network B can reduce the unmet demand, this also results in higher network complexity. Considering the RR instances shown in Tables 10 and 11, we see a similar range of resilience scores for a range of fixed costs that are much higher in RR_{AB}. However, in the RH problem instances, expanding A and B together may be beneficial if maximum resilience is of concern. Since the hub-and-spoke structure is

vulnerable to critical node disruptions, adding more supply (hub) nodes in B would lead to better survivability. Nonetheless, adding hub nodes generally requires their corresponding spoke nodes to be established which results in a higher cost.

The Pareto optimal solutions for the RR_A and RR_{AB} instances are presented in Table 10 and Tables 11, respectively. We observe approximately a 10% improvement in resilience score through optimal commodity flow post-disruption alone. In the lowest fixed-cost solutions, the transshipment node $A397$ is opened first in both cases. Since the transshipment node enables more flow with no change to supply and demand, this confirms the importance of having flow connectivity post-disruption. Then for the next incremental-cost solutions including the TOPSIS solutions, the supply nodes of A are added to improve the resilience score. We note that the supply nodes of A that do not depend on commodity b are preferred to avoid the addition of the interdependent links $B-A$ and the flow cost of b. As more demand nodes of A are added, we observe a gradual drop in the resilience score which indicates a diminishing rate of return on higher-cost solutions. For the RR_{AB} instance, the addition of candidate B components is associated with the higher total cost. Adding the supply nodes of B can reduce the unmet demand; however, it also incurs the cost of the interdependent links $A-B$ and the cost of transporting commodity a. We see that adding the interdependent supply nodes can improve resilience, however, they are often not the most economical choice.

For the RH instances, the Pareto optimal solutions are summarized in Table 12 to Table 14. It is observed that the unmet demand of a cannot be reduced by optimizing the commodity flow alone and candidate A nodes need to be open. For RH_A (Table 12), three demand nodes ($A379$, $A385$, and $A386$) are opened in the lower cost solutions to enable additional service captured and optimal flow. Then, in the TOPSIS solution with the next cost increment, the resilience gain diminishes as only the supply node $A359$ is open. For the expanded network in the instance RH_{AB}, the supply node $A359$ is immediately open first in the lower-cost solutions (including the TOPSIS solution) before the demand nodes $A379$ and $A385$ are added in the next higher-cost solution. For network B expansion in RH_B, a resilience improvement of approximately 12% can be attained through the optimal flow of commodity b alone. Expanding the hub-and-spoke network B proved to have a limited impact on the overall resilience score of interdependent networks.

In all five instances, we observe that the majority of candidate components selected in the lower total cost solutions are a subset of those selected in the highest total cost solutions. Similarly, most of the candidate components that are open in A-only or B-only expansions are also a subset of those open in both A and B expansions. In networks RR_{AB} and RH_{AB}, the highest cost solutions (solution number 20) in both cases have a similar number of candidate components added for comparable fixed costs. However, the differing resilience scores provide strong evidence of a topology effect, i.e., network RR_{AB} is more resilient than RH_{AB} when fully expanded subject to the set of disruption scenarios. Further, we find that lower-cost candidate components are not favored over the higher-cost ones. Candidates with higher supply or higher demand are not more likely to be added. Also for candidate links, the candidate-to-candidate type links are less likely to be selected in the low-cost solutions.

Table 10: Pareto optimal solutions for RR_A instance.

Solution Number	1	2	3	4	5	6	7	8	9*	10	11	12	13	14	15	16	17	18	19	20
Total cost[1]	296	307	319	334	351	369	478	498	531	627	719	754	822	1,031	1,329	1,633	1,987	2,387	2,970	4,520
Resilience score[1]	0.510	0.498	0.485	0.473	0.461	0.449	0.436	0.424	0.412	0.399	0.387	0.375	0.362	0.350	0.338	0.326	0.313	0.301	0.289	0.276
Fixed cost	-	-	-	-	-	-	98	98	106	196	278	294	346	546	836	1,124	1,463	1,851	2,419	3,954
Flow cost[1]	296	307	319	334	351	369	380	399	425	431	441	460	475	485	493	509	525	536	552	566
Network complexity[2]	0.00%	0.00%	0.00%	0.00%	0.00%	0.00%	0.23%	0.23%	0.23%	0.17%	0.35%	0.40%	0.52%	0.98%	1.33%	2.01%	2.35%	3.16%	4.41%	7.04%
Unmet demand[1,3]	60.0%	58.6%	57.1%	55.7%	54.2%	52.8%	51.3%	49.8%	48.4%	47.0%	45.5%	44.0%	42.6%	41.0%	39.5%	38.0%	36.4%	34.9%	33.2%	31.3%
Candidate nodes open							1	1	1	1	1	2	2	4	5	9	10	13	20	32
Supply A										1	1	1	1	1	2	2	3	3	3	5
Transshipment A							1	1	1			1	1	1	2	2	3	4	9	15
Demand A														2	1	5	4	6	8	12
Candidate links open							2	2	2	1	4	3	5	9	13	17	21	29	37	59
$A-A$							2	2	2	1	4	3	5	9	12	16	20	28	36	57
$B-A$															1	1	1	1	1	2

* TOPSIS solution, [1] Expected value, [2] Unscaled value from candidate A and B components only, [3] Unscaled value from commodities a and b

Table 11: Pareto optimal solutions for RR_{AB} instance.

Solution Number	1	2	3	4	5	6	7	8	9	10	11*	12	13	14	15	16	17	18	19	20
Total cost[1]	310	322	338	357	378	486	510	616	684	747	795	961	1,277	1,549	1,911	2,276	2,733	3,350	4,084	5,728
Resilience score[1]	0.510	0.497	0.485	0.472	0.460	0.447	0.435	0.422	0.410	0.397	0.384	0.372	0.359	0.347	0.334	0.322	0.309	0.297	0.284	0.271
Fixed cost	-	-	-	-	-	98	98	196	248	294	321	476	776	1,029	1,377	1,726	2,167	2,771	3,483	5,115
Flow cost[1]	310	322	338	357	378	388	412	420	436	453	474	485	501	520	534	550	567	579	601	613
Network complexity[2]	0.00%	0.00%	0.00%	0.00%	0.00%	0.22%	0.22%	0.16%	0.28%	0.38%	0.44%	0.78%	1.43%	1.66%	2.10%	2.81%	3.75%	4.78%	5.93%	8.57%
Unmet demand[1,3]	60.0%	58.5%	57.0%	55.6%	54.1%	52.6%	51.1%	49.6%	48.1%	46.6%	45.2%	43.6%	42.0%	40.5%	39.0%	37.3%	35.7%	34.0%	32.4%	30.4%
Candidate nodes open						1	1	1	1	2	2	3	7	7	9	13	17	23	29	42
Supply A								1	1	1	1	1	1	2	3	3	3	3	3	5
Transshipment A						1	1			1	1	1	1	2	2	3	6	8	9	15
Demand A												1	4	1	2	5	6	7	9	12
Supply B																		1	2	2
Transshipment B														1	1	1	1	1	2	3
Demand B													1	1	1	1	1	3	4	5
Candidate links open						2	2	1	3	3	4	8	12	16	20	25	34	41	50	72
$A-A$						2	2	1	3	3	4	8	11	12	16	21	30	34	39	58
$A-B$																		1	2	2
$B-B$													1	3	3	3	3	5	8	10
$B-A$														1	1	1	1	1	1	2

* TOPSIS solution, [1] Expected value, [2] Unscaled value from candidate A and B components only, [3] Unscaled value from commodities a and b.

Table 12: Pareto optimal solutions for RH_A instance.

Solution Number	1	2	3	4	5	6	7	8	9	10*	11	12	13	14	15	16	17	18	19	20
Total cost[1]	540	544	547	550	554	559	566	573	583	601	669	884	1,074	1,267	1,478	1,743	1,988	2,259	2,657	3,608
Resilience score[1]	0.511	0.504	0.497	0.490	0.484	0.477	0.470	0.463	0.456	0.450	0.443	0.436	0.429	0.422	0.416	0.409	0.402	0.395	0.388	0.382
Fixed cost	245	245	245	245	245	245	245	245	245	253	310	521	701	891	1,090	1,347	1,585	1,845	2,236	3,180
Flow cost[1]	295	298	302	305	309	314	321	328	338	349	360	364	373	377	388	396	403	413	421	428
Network complexity[2]	0.58%	0.58%	0.58%	0.58%	0.58%	0.58%	0.58%	0.58%	0.58%	0.29%	0.42%	0.93%	1.34%	1.40%	1.80%	2.10%	2.67%	3.26%	4.12%	5.81%
Unmet demand[1,3]	60.0%	59.2%	58.4%	57.6%	56.8%	56.0%	55.2%	54.4%	53.6%	52.8%	52.0%	51.1%	50.3%	49.5%	48.6%	47.7%	46.8%	45.9%	45.0%	43.9%
Candidate nodes open	3	3	3	3	3	3	3	3	3	1	1	4	6	6	8	9	12	14	19	26
Supply A										1	1	1	1	2	2	3	3	3	3	4
Transshipment A															1	2	3	5	8	12
Demand A	3	3	3	3	3	3	3	3	3			3	5	4	5	4	6	6	8	10
Candidate links open	4	4	4	4	4	4	4	4	4	3	5	8	11	12	15	18	22	28	33	48
$A-A$	4	4	4	4	4	4	4	4	4	3	5	8	11	12	15	17	21	27	32	47
$B-A$																1	1	1	1	1

* TOPSIS solution, [1] Expected value, [2] Unscaled value from candidate A and B components only, [3] Unscaled value from commodities a and b

Table 13: Pareto optimal solutions for RH_B instance.

Solution Number	1	2	3	4	5	6	7	8	9	10*	11	12	13	14	15	16	17	18	19	20
Total cost[1]	269	271	273	276	281	285	290	294	299	305	311	318	325	335	596	604	685	775	1,068	1,223
Resilience score[1]	0.510	0.505	0.501	0.496	0.492	0.487	0.482	0.478	0.473	0.468	0.464	0.459	0.455	0.450	0.445	0.441	0.436	0.431	0.427	0.422
Fixed cost	-	-	-	-	-	-	-	-	-	-	-	-	-	-	259	259	330	417	701	849
Flow cost[1]	269	271	273	276	281	285	290	294	299	305	311	318	325	335	337	346	355	359	367	374
Network complexity[2]	0.00%	0.00%	0.00%	0.00%	0.00%	0.00%	0.00%	0.00%	0.00%	0.00%	0.00%	0.00%	0.00%	0.00%	0.25%	0.25%	0.44%	0.62%	1.06%	1.43%
Unmet demand[1,3]	60.0%	59.5%	58.9%	58.4%	57.8%	57.3%	56.7%	56.2%	55.6%	55.1%	54.6%	54.0%	53.5%	52.9%	52.3%	51.8%	51.2%	50.6%	50.0%	49.4%
Candidate nodes open															1	1	2	3	5	7
Supply B															1	1	1	1	2	2
Transshipment B																			1	1
Demand B																	1	2	2	4
Candidate links open															2	2	3	4	7	9
$A-B$															1	1	1	1	2	2
$B-B$															1	1	2	3	5	7

* TOPSIS solution, [1] Expected value, [2] Unscaled value from candidate A and B components only, [3] Unscaled value from commodities a and b

Table 14: Pareto optimal solutions for RH_{AB} instance.

Solution Number	1	2	3	4	5	6*	7	8	9	10	11	12	13	14	15	16	17	18	19	20
Total cost[1]	583	588	595	603	615	634	841	1,021	1,254	1,481	1,711	1,954	2,223	2,504	2,803	3,126	3,507	3,983	4,589	5,630
Resilience score[1]	0.511	0.502	0.494	0.486	0.478	0.470	0.462	0.454	0.446	0.438	0.430	0.422	0.414	0.405	0.397	0.389	0.381	0.373	0.365	0.357
Fixed cost	280	280	280	280	280	280	478	650	871	1,087	1,306	1,543	1,800	2,070	2,359	2,671	3,041	3,510	4,107	5,142
Flow cost[1]	304	308	315	323	335	354	364	371	384	394	405	411	422	434	445	456	466	473	481	488
Network complexity[2]	0.34%	0.34%	0.34%	0.34%	0.34%	0.34%	0.78%	0.84%	1.33%	1.45%	1.93%	2.16%	2.70%	3.15%	3.59%	4.19%	5.08%	5.79%	6.87%	8.58%
Unmet demand[1,3]	60.0%	59.0%	58.1%	57.1%	56.2%	55.2%	54.2%	53.3%	52.2%	51.2%	50.2%	49.2%	48.2%	47.1%	46.1%	45.1%	43.9%	42.9%	41.7%	40.5%
Candidate nodes open	1	1	1	1	1	1	3	3	6	6	9	10	13	15	17	20	24	28	35	43
Supply A	1	1	1	1	1	1	1	1	1	1	1	2	2	2	3	3	3	3	3	4
Transshipment A														1	2	4	6	6	8	12
Demand A							2		3	1	3	3	4	4	5	6	7	7	8	10
Supply B								1	1	2	2	2	2	2	2	2	2	3	4	4
Transshipment B										1	1	1	1	1	1	1	1	1	1	1
Demand B								1	1	1	2	2	4	5	4	4	5	8	11	12
Candidate links open	4	4	4	4	4	4	8	9	12	14	17	19	23	27	31	36	44	49	55	70
$A-A$	4	4	4	4	4	4	8	5	8	6	8	10	11	14	18	23	30	31	33	47
$A-B$								2	2	3	3	3	3	3	3	3	3	4	5	5
$B-B$								2	2	5	6	6	9	10	9	9	10	13	16	17
$B-A$															1	1	1	1	1	1

* TOPSIS solution, [1] Expected value, [2] Unscaled value from candidate A and B components only, [3] Unscaled value from commodities a and b

The results for the TOPSIS solutions from five problem instances are presented in Table 15. We observe a maximum of two candidate nodes A and four candidate links $A-A$ open in five TOPSIS instances. Since this is a minor addition to the total number of existing nodes and links, the contribution of network complexity in the resilience score is marginal. Hence, the resilience score is heavily influenced by the unmet demand in all cases. We observe that the supply node $A359$ is added in all instances with A expansion. Notably, this supply node is not an interdependent node, i.e., it is not a demand node for commodity b. This suggests a strategy to open candidate nodes that improve network supply without increasing the unmet demand. For the RR_A and RR_{AB} instances, the transshipment node $A397$ is added to enable an additional flow path from the existing supply node $A32$. Due to their low fixed-cost advantage, adding the candidate transshipment nodes can help improve the connectivity and the ability to meet demand. Since none of network B components are opened, we see that focusing the expansion on the larger network A would be more appropriate.

Considering the expanded networks' serviceability post-disruption, the service levels of commodity a are within the same magnitude across instances. However, the service levels of commodity b are lower in RH instances than those of RR instances. This implies that hub-and-spoke topology negatively impacts the ability to meet demand when compared with random topology. We find that random topology affords more flexibility in flow paths between supply and demand nodes and makes better utilization of routes with available link capacities. Therefore, a topological structure with strong network connectivity post-disruption forms a foundation for improved resilience.

The graph metrics of the random and hub-and-spoke networks were determined according to Table 4 to quantify the topology effect on resilience. While the maximum node degree and network diameter provide the maximum network statistics as the upper bounds, they are not helpful for describing the overall change in heterogeneous network connectivity. This particularly applies to network expansion where the added candidate nodes and links may not change the maximum degree or diameter. In Table 15, the lowest average node degree is seen in Hub-and-spoke B due to a large number of direct supply-demand links. Additionally, the average clustering coefficient, a measure of how well connected each node is within its neighborhood, is lower in Hub-and-spoke B than its random counterparts. Since most of the demand nodes in Hub-and-spoke B are allocated to one single supply node, the number of triangles in the graph is lower as a result. This low-cluster property reflects a scale-free characteristic. For the average shortest path length, Hub-and-spoke B has the highest value which indicates that commodity b has longer physical flow paths to reach its demand nodes on average. This is confirmed by the unmet demands of b in the RH instances being several times larger than those of the RR instances. Based on these observations, resilient interdependent networks with good connectivity can be characterized as having a high average node degree, high clustering coefficient, and low average shortest path length.

Figure 7 shows the distribution of network characteristics, i.e., node degree, clustering coefficient, and shortest path length of the five TOPSIS expanded networks separated by commodity. The distributions are computed using kernel density estimation to show continuous data for visualization purposes [102]. Within

Table 15: TOPSIS solutions of the expanded networks with critical node disruptions.

Instance	RR_A		RR_{AB}		RH_A		RH_B		RH_{AB}	
Pareto solution number	9		11		10		10		6	
Objectives: (Obj. 1, Obj. 2)	(530.6, 0.4117)		(794.7, 0.3845)		(601.3, 0.4496)		(304.5, 0.4684)		(633.8, 0.4701)	
Network topology	Random	Random	Random	Random	Random	Hub&Spoke	Random	Hub&Spoke	Random	Hub&Spoke
Network (Commodity)	A (a)	B (b)	A (a)	B (b)	A (a)	B (b)	A (a)	B (b)	A (a)	B (b)
Expansion	Yes	No	Yes	Yes	Yes	No	No	Yes	Yes	Yes
Candidate components open										
Candidate nodes	1: A397^o	N/A	2: A359^s, A397^o	0	1: A359^s	N/A	N/A	0	1: A359^s	0
Candidate links	2: (A32^s, A397^o), (A397^o, A78^t)	N/A	4: (A359^s, A110^t), (A359^s, A252^t), (A32^s, A397^o), (A397^o, A339^o)	0	3: (A359^s, A110^t), (A359^s, A200^t), (A359^s, A242^t)	N/A	N/A	0	4: (A359^s, A110^t), (A359^s, A200^t), (A359^s, A242^t), (A359^s, A252^t)	0
Breakdown of objective function values and service levels										
Obj. 1 Expected total cost	375.5	155.1	602.4	192.3	499.6	101.7	207.3	97.2	532.1	101.7
Fixed cost^C	105.9	0.0	320.8	0.0	252.8	0.0	0.0	0.0	279.7	0.0
Expected flow cost^A	269.6	155.1	281.6	192.3	246.8	101.7	207.3	97.2	252.4	101.7
Obj. 2 Expected resilience score	0.3512	0.0604	0.3284	0.0560	0.3601	0.0896	0.3324	0.1360	0.3429	0.1272
Network complexity^{S,C}	0.0003	0.0000	0.0007	0.0000	0.0004	0.0000	0.0000	0.0000	0.0005	0.0000
Expected unmet demand^{S,A}	0.3509	0.0604	0.3278	0.0560	0.3596	0.0896	0.3324	0.1360	0.3424	0.1272
Expected service level	46.6%	68.6%	48.8%	73.4%	41.9%	61.3%	41.7%	51.4%	41.9%	51.2%
Network characteristics										
Total number of nodes	355	56	356	56	355	56	354	56	355	56
Total number of links	546	155	548	155	546	133	543	133	547	133
Avg. node degree	3.020	3.100	3.028	3.100	3.025	2.687	3.017	2.687	3.030	2.687
Max. node degree	13	10	13	10	13	12	13	12	13	12
Network diameter*	10	9	10	9	10	7	10	7	10	7
Avg. clustering coefficient**	0.1500	0.1739	0.1533	0.1739	0.1494	0.0278	0.1493	0.0278	0.1521	0.0278
Avg. shortest path length†	0.6098	0.5998	0.6102	0.5998	0.6107	0.6961	0.6113	0.6961	0.6106	0.6961

Node type: s = supply, o = transshipment, and t = demand nodes. Basis of calculation: S = scaled values, C = candidate component only, A = all existing and candidate components, * = Directed graph. ** = Undirected, unweighted graph. † Directed, weighted graph (weight='length'), based on each commodity.

the RR and RH instances, we are unable to distinguish the differences between expansion opportunities (A, B, or both) due to the small number of candidate components added. However, between the random and hub-and-spoke topologies of the RR and RH instances, we observe distinct patterns.

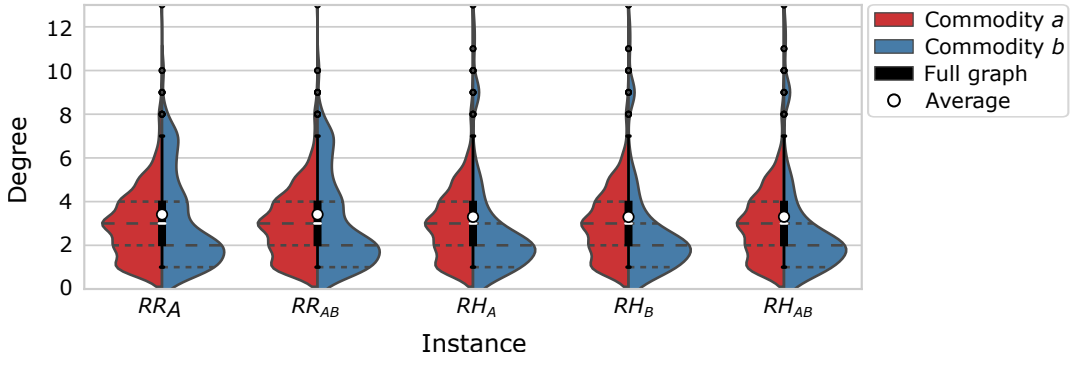

(a) Node degree distribution.

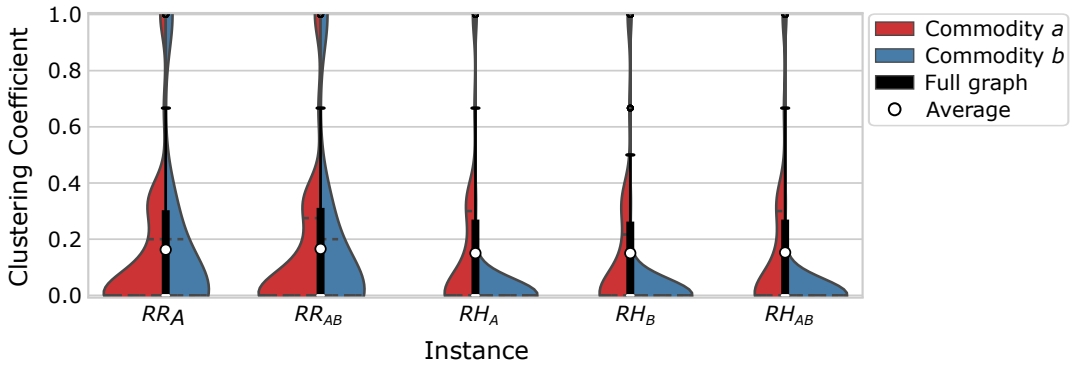

(b) Local clustering coefficient distribution

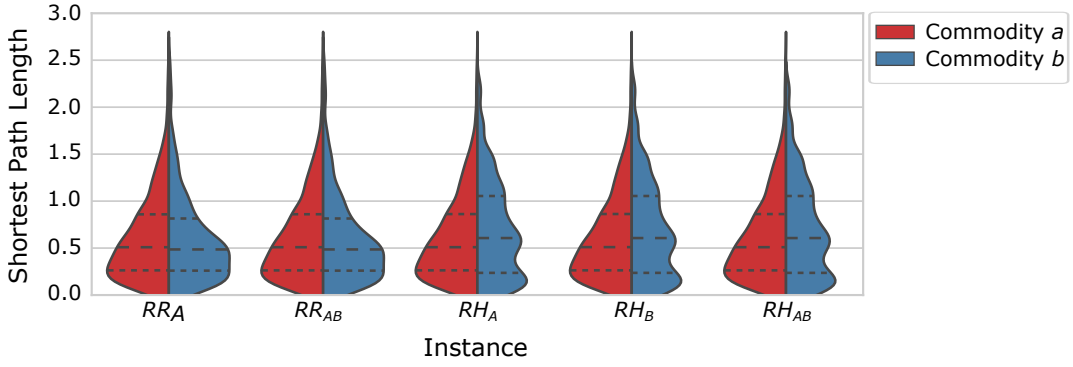

(c) Shortest path length distribution

Figure 7: Network characteristics of the TOPSIS solutions with critical node disruptions. The dashed lines indicate the median and interquartile range of the estimated distribution. The middle box plots display the distribution of the average values for the full graph if applicable.

In Figure 7a, the node degree distributions in all instances exhibit a long-tailed property commonly found in heterogeneous network structures [14]. This is congruent with many real-world complex networks where most nodes have a small degree and a few nodes have a relatively high degree. Network Random A with commodity a exhibits an exponential degree distribution that is commonly present in a random graph. For Random B (RR instances), a higher proportion of nodes with a degree ≥ 6 are observed due to the inclusion

of interdependent links $B - A$. Most nodes of Hub-and-spoke B (RH instances) have a relatively small degree with the exception of supply (hub) nodes having a high node degree of 9.

In Figure 7b, we observe that networks Random A and Random B contain nodes with a maximum clustering coefficient of 1. These nodes are fully connected to their neighbors since links are randomly connected to the nodes in the random graph regardless of the node type. In contrast, most nodes in Hub-and-spoke B have a minimum clustering coefficient of 0, i.e., the neighboring spoke nodes are not directly connected to each other. This leads to the RH instances having less network connectivity than the RR instances on average.

The distribution of shortest path lengths in Figure 7c displays a long-tail characteristic in five instances. The distributions of Random A and Random B (RR instances) are almost symmetrical since they share the same topology with more than half of the shortest path lengths being less than 0.5. On the other hand, most of the shortest path lengths in Hub-and-spoke B (RH instances) are longer than 0.5 due to the multi-segment travel between hubs.

Based on these findings, we see that interdependent networks with a hub-and-spoke structure are more vulnerable to disruptions involving critical supply nodes. Their network nodes are less connected with the potential to limit the service level. Additionally, the commodity flow cost can be higher due to the longer shortest path lengths. Considering the full graph with both commodities, the network characteristics of all five instances resemble more closely to an ER random graph. However, we observe the scale-free attribute in the node degree distribution as the network expands. This is due to the preferential attachment behavior in which candidate nodes are more likely to attach to the more connected nodes. The results in this study are generalized based on the relative comparison between heterogeneous interdependent networks with random and hub-and-spoke structures under critical node disruptions. The research findings cannot be extended to networks with other topologies and further analysis will be required.

6. Discussion and Lessons Learned

The major findings from our research can support resilience optimization strategy for interdependent networks through network expansion. From the evaluation of the network topology effect on resilience improvement under disruption uncertainty, we derive the following key insights.

i **Heterogeneous network instance generation**: The network instance generation demonstrates the difficulty in controlling the topology of heterogeneous networks to be purely random, scale-free, or small-world, especially when the network increases in size. In a directed network where the flow of commodities must make physical or logical sense, it remains a challenge to fine-tune one property of graph metrics without affecting another. While graph metrics can help to identify unique characteristics of certain well-established graph models, individual graph metrics alone prove inadequate to identify network topologies. Real-world CIs are highly complex and highly

heterogeneous possessing characteristics of many different topologies, and functional relationships between network components must be incorporated to make meaningful network expansion decisions.

ii **Disruption scenario generation and scenario reduction**: Our resilience optimization model is a stochastic programming problem that determines network expansion decisions under uncertainty. Resilience outcome depends on the disruptions that are unpredictable in nature, and scenario reduction helps to manage computational complexity and solution time limitations. In the stochastic optimization model, discrete approximations of the random data are employed to incorporate uncertain parameters with known probabilities. For the deterministic equivalent problem to be practical computationally, it is often necessary to reduce the problem size by limiting the number of scenarios to represent the significant ones.

iii **Topology effect on the network expansion decision**: Our network expansion decisions are the ones that optimize the expected total cost and expected resilience objectives under critical node disruptions. For a similar expected total cost, the opportunity to improve resilience is greater in random networks than in hub-and-spoke topology which is more vulnerable to hub failures. Networks with better flow connectivity are more resilient, thus the transshipment node and links are good candidates to open if they have the cost advantage over other node types. Adding interdependent nodes can help improve resilience but the need for infrastructure support for external commodities presents a cost trade-off. The candidate components selected in the lower total cost solutions are a subset of those selected in the highest total cost solutions. This presents an opportunity for multi-stage expansion where additional candidates can be opened when more expansion budget becomes available.

iv **Characterization of expanded network topologies**: Although no single graph metrics can be used to characterize the network graph, common characteristics of a resilient network with high connectivity are high average node degree, high clustering coefficient, and low average shortest path length. CI networks exhibit a scale-free attribute as the network expands due to the preferential attachment behavior, i.e., candidate nodes are more likely to attach to the more connected nodes which already have high node degrees. This may result in increased vulnerability if more components of the expanded networks become more critical and the expansion strategy may need to be adapted.

7. Conclusions and Future Work

To improve the resilience of interdependent critical infrastructure (CI) via network expansion, we need to analyze the functional relationships of heterogeneous networks, the CI's topological structure, and the nature of disruptive events. In this work, we propose the evaluation of the network topology effect on the resilience of interdependent CIs under critical node disruptions. Based on our stochastic multi-objective resilience optimization model, we determine optimal network expansion decisions that satisfy the conflicting

objectives of total cost and resilience score post-disruption. The resilience score is quantified from the network complexity and the unmet demand metrics.

We develop a method to generate network graphs of two interacting CIs containing random and hub-and-spoke (i.e., clustering) topologies. Once critical node disruption scenarios are generated, scenario reductions are performed to reduce the problem size and computational complexity. For each problem instance, we apply a two-stage stochastic programming approach to our resilience optimization model. The first-stage decisions are the optimal locations of candidate nodes and links to open. The second-stage decisions relate to the optimal flow allocation, the unmet demand, and the unused supply post-disruption. Our study shows that resilience post-disruption can be improved in expanded networks. However, resilience improvement is more limited in interdependent networks where the hub-and-spoke structure is present. Random network topology is found to be better connected than the hub-and-spoke topology due to a higher average node degree, higher average clustering coefficient, and lower average shortest path. Since a network with strong connectivity positively contributes to lowering the unmet demand, random network characteristics are more resilient to critical node disruption. This finding confirms that a scale-free characteristic of the hub-and-spoke structures makes them vulnerable to targeted attacks.

The resilience evaluation completed in this study can be extended to incorporate interdependent networks with different topologies in future research. Alternative strategies for scenario generation can be incorporated to cover a wider range of scenario space. Further, an additional combination of networks and commodities can be explored to analyze interdependent network resilience from the true perspective of networks of networks [14, 31, 66]. Although we are able to obtain exact solutions without computational difficulty, the complexity of the problem instances will grow with the network size and the number of stochastic scenarios considered. The problem characteristics for highly complex CIs can also affect the solution time regardless of the problem size. Solution techniques are often exploited from the underlying structure of the problem which likely requires different strategies between network topologies and disruption types. Further analysis of the solution insights that can support the future development of heuristic approaches for this problem should be explored.

References

[1] S. M. Rinaldi, J. P. Peerenboom, T. K. Kelly, Identifying, Understanding, and Analyzing Critical Infrastructures Interdependencies, IEEE Control Systems Magazine (2001) 11–25.
URL http://ieeexplore.ieee.org/document/1265180/

[2] P. Pederson, D. Dudenhoeffer, S. Hartley, M. Permann, Critical Infrastructure Interdependency Modeling: A Survey of U.S. and International Research, Tech. rep., Idaho National Laboratory, Idaho Falls, Idaho (2006).
URL http://www.osti.gov/servlets/purl/911792-X4IFHO/

[3] R. Setola, V. Rosato, E. Kyriakides, E. Rome, Managing the Complexity of Critical Infrastructures:

A Modelling and Simulation Approach, Studies in Systems, Decision and Control, Springer Nature, 2016.
URL http://www.springer.com/series/13304

[4] S. Mukherjee, R. Nateghi, M. Hastak, A multi-hazard approach to assess severe weather-induced major power outage risks in the U.S., Reliability Engineering & System Safety 175 (2018) 283–305.

[5] The Texas Tribune, Gov. Greg Abbott wants power companies to "winterize." Texas' track record won't make that easy., https://www.texastribune.org/2021/02/20/texas-power-grid-winterize/, [Online; accessed April 16, 2021] (2021).

[6] T. C. Sharkey, S. G. Nurre, H. Nguyen, J. H. Chow, J. E. Mitchell, W. A. Wallace, Identification and Classification of Restoration Interdependencies in the Wake of Hurricane Sandy, Journal of Infrastructure Systems 22 (1) (2016) 04015007.

[7] K. Tierney, M. Bruneau, Conceptualizing and Measuring Resilience - A Key to Disaster Loss Reduction, TR News 250 (2007) 14–18.
URL http://onlinepubs.trb.org/onlinepubs/trnews/trnews250_p14-17.pdf

[8] D. Henry, J. E. Ramirez-Marquez, Generic metrics and quantitative approaches for system resilience as a function of time, Reliability Engineering & System Safety 99 (2012) 114–122.
URL http://dx.doi.org/10.1016/j.ress.2011.09.002

[9] R. Francis, B. Bekera, A metric and frameworks for resilience analysis of engineered and infrastructure systems, Reliability Engineering & System Safety 121 (2014) 90–103.
URL http://dx.doi.org/10.1016/j.ress.2013.07.004

[10] C. Nan, G. Sansavini, A quantitative method for assessing resilience of interdependent infrastructures, Reliability Engineering & System Safety 157 (2017) 35–53.
URL http://dx.doi.org/10.1016/j.ress.2016.08.013

[11] A. J. Hickford, S. P. Blainey, A. Ortega Hortelano, R. Pant, Resilience engineering: theory and practice in interdependent infrastructure systems, Environment Systems and Decisions 38 (3) (2018) 278–291.
URL http://dx.doi.org/10.1007/s10669-018-9707-4

[12] M. Barthélemy, Spatial Networks, Physics Reports 499 (1-3) (2011) 1–101.
URL http://dx.doi.org/10.1016/j.physrep.2010.11.002

[13] R. G. Morris, M. Barthélemy, Transport on coupled spatial networks, Physical Review Letters 109 (12) (2012) 2–5.

[14] L. D. Valdez, L. Shekhtman, C. E. La Rocca, Z. Zhang, S. V. Buldyrev, P. A. Trunfio, L. A. Braunstein, H. Shlomo, Cascading Failures in Complex Networks, Journal of Complex Networks 8 (2) (2020) 1–25. URL https://doi.org/10.1093/comnet/cnaa013

[15] T. McDaniels, S. E. Chang, D. Cole, J. Mikawoz, H. Longstaff, Fostering resilience to extreme events within infrastructure systems: Characterizing decision contexts for mitigation and adaptation, Global Environmental Change 18 (2) (2008) 310–318.

[16] A. R. Ganguly, U. Bhatia, S. E. Flynn, U. Bhatia, S. E. Flynn, Critical Infrastructures Resilience, Policy and Engineering Principles, Taylor & Francis, New York, NY, 2018.
URL https://doi.org/10.4324/9781315153049

[17] A. Tiong, H. A. Vergara, Multi-Objective Resilience Optimization for Interdependent Critical Infrastructure Network Expansion, unpublished (2021).

[18] A. Tiong, H. A. Vergara, International Journal of Critical Infrastructure Protection A two-stage stochastic multi-objective resilience optimization model for network expansion of interdependent power – water networks under disruption, International Journal of Critical Infrastructure Protection 40 (January) (2023) 100588.
URL https://doi.org/10.1016/j.ijcip.2023.100588

[19] M. A. Di Muro, L. D. Valdez, H. H. Aragão Rêgo, S. V. Buldyrev, H. E. Stanley, L. A. Braunstein, Cascading Failures in Interdependent Networks with Multiple Supply-Demand Links and Functionality Thresholds, Scientific Reports 7 (1) (2017) 1–10.

[20] K. Zhao, A. Kumar, T. P. Harrison, J. Yen, Analyzing the resilience of complex supply network topologies against random and targeted disruptions, IEEE Systems Journal 5 (1) (2011) 28–39.

[21] A. T. Murray, An overview of network vulnerability modeling approaches, GeoJournal 78 (2) (2013) 209–221.

[22] M. Ouyang, Review on modeling and simulation of interdependent critical infrastructure systems, Reliability Engineering & System Safety 121 (2014) 43–60.
URL http://dx.doi.org/10.1016/j.ress.2013.06.040

[23] M. Ghosn, L. Dueñas-Osorio, D. M. Frangopol, T. P. McAllister, P. Bocchini, L. Manuel, B. R. Ellingwood, S. Arangio, F. Bontempi, M. Shah, M. Akiyama, F. Biondini, S. Hernandez, G. Tsiatas, Performance Indicators for Structural Systems and Infrastructure Networks, Journal of Structural Engineering 142 (9) (2016) 1–18.

[24] M. Ouyang, L. Hong, Z. Mao, M.-H. Yu, F. Qi, A methodological approach to analyze vulnerability of interdependent infrastructures, Simulation Modelling Practice and Theory 17 (5) (2009) 817–828.
URL http://dx.doi.org/10.1016/j.simpat.2009.02.001

[25] M. Ouyang, L. Zhao, Do topological models contribute to decision making on post-disaster electric power system restoration?, Chaos: An Interdisciplinary Journal of Nonlinear Science 24 (4) (2014) 043131.

[26] P. D. H. Hines, E. Cotilla-Sanchez, S. Blumsack, Do topological models provide good information about electricity infrastructure vulnerability?, Chaos: An Interdisciplinary Journal of Nonlinear Science 20 (3) (2010) 1–5.

[27] S. Y. Lin, S. El-Tawil, Time-Dependent Resilience Assessment of Seismic Damage and Restoration of Interdependent Lifeline Systems, Journal of Infrastructure Systems 26 (1) (2020) 1–13.

[28] L. Dueñas-Osorio, J. I. Craig, B. J. Goodno, Probabilistic response of interdependent infrastructure networks, in: 2nd Annual Meeting of the Asian-Pacific Network of Centers for Earthquake Engineering Research (ANCER), Honolulu, HI, 2004, p. 28–30.
URL http://citeseerx.ist.psu.edu/viewdoc/download?doi=10.1.1.123.2036&rep=rep1&type=pdf

[29] A. Rose, Economic resilience to natural and man-made disasters: Multidisciplinary origins and contextual dimensions, Environmental Hazards 7 (2007) 383–398.

[30] R. Pant, K. Barker, C. W. Zobel, Static and dynamic metrics of economic resilience for interdependent infrastructure and industry sectors, Reliability Engineering & System Safety 125 (2014) 92–102.

[31] J. Gao, X. Liu, D. Li, S. Havlin, Recent progress on the resilience of complex networks, Energies 8 (10) (2015) 12187–12210.

[32] X. Liu, E. Ferrario, E. Zio, Resilience Analysis Framework for Interconnected Critical Infrastructures, ASCE-ASME J. Risk and Uncert. in Engrg. Sys., Part B: Mech. Engrg. 3 (2) (2017) 021001.

[33] N. Haghighi, S. K. Fayyaz, X. C. Liu, T. H. Grubesic, R. Wei, A Multi-Scenario Probabilistic Simulation Approach for Critical Transportation Network Risk Assessment, Networks and Spatial Economics 18 (1) (2018) 181–203.

[34] G. Byeon, P. Van Hentenryck, R. Bent, H. Nagarajan, Communication-Constrained Expansion Planning for Resilient Distribution Systems, INFORMS Journal on Computing 32 (4) (2020) 968–985.
URL https://doi.org/10.1287/ijoc.2019.0899

[35] A. D. González, L. Dueñas-Osorio, M. Sánchez-Silva, A. L. Medaglia, The Interdependent Network Design Problem for Optimal Infrastructure System Restoration, Computer-Aided Civil and Infrastructure Engineering 31 (5) (2016) 334–350.

[36] Q. Mao, N. Li, Assessment of the impact of interdependencies on the resilience of networked critical infrastructure systems, Natural Hazards 93 (1) (2018) 315–337.
URL https://doi.org/10.1007/s11069-018-3302-3

[37] Y. Almoghathawi, K. Barker, L. A. Albert, Resilience-driven restoration model for interdependent infrastructure networks, Reliability Engineering & System Safety 185 (December 2018) (2019) 12–23.
URL https://doi.org/10.1016/j.ress.2018.12.006

[38] Y. Fang, G. Sansavini, Optimum post-disruption restoration under uncertainty for enhancing critical infrastructure resilience, Reliability Engineering & System Safety 185 (December 2018) (2019) 1–11.
URL https://doi.org/10.1016/j.ress.2018.12.002

[39] S. Hosseini, K. Barker, J. E. Ramirez-Marquez, A review of definitions and measures of system resilience, Reliability Engineering & System Safety 145 (2016) 47–61.

[40] T. Afrin, N. Yodo, Towards Resilient Interdependent Networks with a Hybrid Recovery Framework, in: L. Cromarty, R. Shirwaiker, P. Wang (Eds.), 2020 IISE Annual Conference, 2020, pp. 91–96.

[41] Y. Almoghathawi, K. Barker, Restoring Community Structures in Interdependent Infrastructure Networks, IEEE Transactions on Network Science and Engineering (2019) 1–1.
URL https://ieeexplore.ieee.org/document/8758788/

[42] D. B. Karakoc, Y. Almoghathawi, K. Barker, A. D. González, S. Mohebbi, Community resilience-driven restoration model for interdependent infrastructure networks, International Journal of Disaster Risk Reduction 38 (2019) 101228.
URL https://doi.org/10.1016/j.ijdrr.2019.101228

[43] Y. Almoghathawi, K. Barker, Component importance measures for interdependent infrastructure network resilience, Computers and Industrial Engineering 133 (2019) 153–164.
URL https://doi.org/10.1016/j.cie.2019.05.001

[44] N. Morshedlou, A. D. González, K. Barker, Work crew routing problem for infrastructure network restoration, Transportation Research Part B: Methodological 118 (2018) 66–89.
URL https://doi.org/10.1016/j.trb.2018.10.001

[45] E. L. Mooney, Y. Almoghathawi, K. Barker, Facility location for recovering systems of interdependent networks, IEEE Systems Journal (2018) 1–11.
URL https://ieeexplore.ieee.org/document/8468026/

[46] M. Zhalechian, S. A. Torabi, M. Mohammadi, Hub-and-spoke network design under operational and disruption risks, Transportation Research Part E: Logistics and Transportation Review 109 (2018) 20–43.
URL http://www.sciencedirect.com/science/article/pii/S1366554517305008

[47] H. Fotouhi, S. Moryadee, E. Miller-Hooks, Quantifying the resilience of an urban traffic-electric power coupled system, Reliability Engineering & System Safety 163 (2017) 79–94.
URL http://dx.doi.org/10.1016/j.ress.2017.01.026

[48] L. Chen, E. Miller-Hooks, Resilience: An Indicator of Recovery Capability in Intermodal Freight Transport, Transportation Science 46 (1) (2012) 109–123.
URL http://pubsonline.informs.org/doi/abs/10.1287/trsc.1110.0376

[49] E. Ibanez, S. Lavrenz, K. Gkritza, D. A. Mejia-Giraldo, V. Krishnan, J. D. McCalley, A. K. Somani, Resilience and robustness in long-term planning of the national energy and transportation system, International Journal of Critical Infrastructures 12 (1/2) (2016) 82–103.
URL http://www.inderscience.com/link.php?id=75869

[50] H. Lobban, Y. Almoghathawi, N. Morshedlou, K. Barker, Community vulnerability perspective on robust protection planning in interdependent infrastructure networks, Proceedings of the Institution of Mechanical Engineers, Part O: Journal of Risk and Reliability 235 (5) (2021) 798–813.

[51] M. Ouyang, A mathematical framework to optimize resilience of interdependent critical infrastructure systems under spatially localized attacks, European Journal of Operational Research 262 (3) (2017) 1072–1084.

[52] B. Adenso-Diaz, C. Mena, S. García-Carbajal, M. Liechty, The impact of supply network characteristics on reliability, Supply Chain Management 17 (3) (2012) 263–276.

[53] M. Falasca, C. W. Zobel, D. Cook, A Decision Support Framework to Assess Supply Chain Resilience, in: F. Fiedrich, B. Van de Walle (Eds.), The 5th International Conference on Information Systems for Crisis Response and Management (ISCRAM), Washington, D. C., 2008, pp. 596–605.

[54] C. W. Craighead, J. Blackhurst, M. J. Rungtusanatham, R. B. Handfield, The severity of supply chain disruptions: Design characteristics and mitigation capabilities, Decision Sciences 38 (1) (2007) 131–156.

[55] G. Fu, S. Wilkinson, R. J. Dawson, A Spatial Network Model for Civil Infrastructure System Development, Computer-Aided Civil and Infrastructure Engineering 31 (9) (2016) 661–680.

[56] F. A. López, A. Páez, J. A. Carrasco, N. A. Ruminot, Vulnerability of nodes under controlled network topology and flow autocorrelation conditions, Journal of Transport Geography 59 (2017) 77–87.
URL http://dx.doi.org/10.1016/j.jtrangeo.2017.02.002

[57] P. D. H. Hines, S. Blumsack, E. Cotilla-Sanchez, C. Barrows, The topological and electrical structure of power grids, Proceedings of the Annual Hawaii International Conference on System Sciences (2010) 1–10.

[58] E. Cotilla-Sanchez, P. D. H. Hines, C. Barrows, S. Blumsack, Comparing the topological and electrical structure of the North American electric power infrastructure, IEEE Systems Journal 6 (4) (2012) 616–626.

[59] S. G. Aksoy, E. Purvine, E. Cotilla-Sanchez, M. Halappanavar, A generative graph model for electrical infrastructure networks, Journal of Complex Networks 7 (1) (2018) 128–162.

[60] M. Ouyang, K. Yang, Does topological information matter for power grid vulnerability?, Chaos: An Interdisciplinary Journal of Nonlinear Science 24 (4) (2014) 043121.

[61] X. Zhang, E. Miller-Hooks, K. Denny, Assessing the role of network topology in transportation network resilience, Journal of Transport Geography 46 (2015) 35–45.
URL http://dx.doi.org/10.1016/j.jtrangeo.2015.05.006

[62] A. Yazdani, R. A. Otoo, P. Jeffrey, Resilience enhancing expansion strategies for water distribution systems: A network theory approach, Environmental Modelling and Software 26 (12) (2011) 1574–1582.
URL http://dx.doi.org/10.1016/j.envsoft.2011.07.016

[63] P. Erd″ os, A. Rényi, On random graphs, Publicationes Mathematicae 6 (1959) 290–297.

[64] D. J. Watts, S. H. Strogatz, Collective dynamics of 'small-world' networks, Nature 393 (June) (1998) 440–442.
URL https://www.ncbi.nlm.nih.gov/pubmed/9623998

[65] A.-L. Barabási, R. Albert, Emergence of scaling in random networks, Science 286 (5439) (1999) 509–512. arXiv:https://science.sciencemag.org/content/286/5439/509.full.pdf.
URL https://science.sciencemag.org/content/286/5439/509

[66] S. Havlin, H. E. Stanley, A. Bashan, J. Gao, D. Y. Kenett, Percolation of interdependent network of networks, Chaos, Solitons and Fractals 72 (2015) 4–19.
URL http://dx.doi.org/10.1016/j.chaos.2014.09.006

[67] L. Cuadra, S. Salcedo-Sanz, J. Del Ser, S. Jiménez-Fernández, Z. W. Geem, A critical review of robustness in power grids using complex networks concepts, Energies 8 (9) (2015) 9211–9265.

[68] X. Fu, P. Pace, G. Aloi, L. Yang, G. Fortino, Topology optimization against cascading failures on wireless sensor networks using a memetic algorithm, Computer Networks 177 (May) (2020) 107327.
URL https://doi.org/10.1016/j.comnet.2020.107327

[69] X. Fu, P. Pace, G. Aloi, W. Li, G. Fortino, Toward robust and energy-efficient clustering wireless sensor networks: A double-stage scale-free topology evolution model, Computer Networks 200 (October)

(2021) 108521.
URL https://doi.org/10.1016/j.comnet.2021.108521

[70] A. Yazdani, P. Jeffrey, A complex network approach to robustness and vulnerability of spatially organized water distribution networks, arXiv preprint arXiv:1008.1770 (2010) 1–18.
URL http://arxiv.org/abs/1008.1770

[71] D. Bienstock, S. Mattia, Using mixed-integer programming to solve power grid blackout problems, Discrete Optimization 4 (1) (2007) 115–141.

[72] S. Pahwa, M. Youssef, C. Scoglio, Electrical Networks: An Introduction, in: G. D'Agostino, A. Scala (Eds.), Networks of Networks: The Last Frontier of Complexity, Springer International Publishing, 2014, Ch. 8, pp. 163–186.

[73] D. Z. Tootaghaj, N. Bartolini, H. Khamfroush, T. L. Porta, Controlling cascading failures in interdependent networks under incomplete knowledge, Proceedings of the IEEE Symposium on Reliable Distributed Systems (2017) 54–63.

[74] V. Rosato, L. Issacharoff, F. Tiriticco, S. Meloni, S. De Porcellinis, R. Setola, Modelling interdependent infrastructures using interacting dynamical models, International Journal of Critical Infrastructures 4 (1-2) (2008) 63–79.

[75] M. Ouyang, Z. Wang, Resilience assessment of interdependent infrastructure systems: With a focus on joint restoration modeling and analysis, Reliability Engineering & System Safety 141 (2015) 74–82.
URL http://dx.doi.org/10.1016/j.ress.2015.03.011

[76] M. H. Amini, O. Karabasoglu, Optimal operation of interdependent power systems and electrified transportation networks, Energies 11 (1) (2018) 1–25.

[77] Q. Zou, S. Chen, Enhancing resilience of interdependent traffic-electric power system, Reliability Engineering & System Safety 191 (February) (2019) 106557.
URL https://linkinghub.elsevier.com/retrieve/pii/S0951832019303102

[78] R. Bent, S. Blumsack, P. van Hentenryck, C. Borraz-Sánchez, S. Backhaus, Joint Expansion Planning for Natural Gas and Electric Transmission with Endogenous Market Feedbacks, in: Proceedings of the 51st Hawaii International Conference on System Sciences, Vol. 9, 2018, pp. 2595–2605.

[79] C. Borraz-Sánchez, R. Bent, S. Backhaus, S. Blumsack, H. Hijazi, P. Van Hentenryck, Convex optimization for joint expansion planning of natural gas and power systems, Proceedings of the Annual Hawaii International Conference on System Sciences (2016) 2536–2545.

[80] Y. Almoghathawi, A. D. González, K. Barker, Exploring Recovery Strategies for Optimal Interdependent Infrastructure Network Resilience, Networks and Spatial Economics (2021) 229–260.

[81] I. Hernandez-Fajardo, L. Dueñas-Osorio, Probabilistic study of cascading failures in complex interdependent lifeline systems, Reliability Engineering & System Safety 111 (2013) 260–272.

[82] W. Zhang, P. Lin, N. Wang, C. D. Nicholson, X. Xue, Probabilistic Prediction of Postdisaster Functionality Loss of Community Building Portfolios Considering Utility Disruptions, Journal of Structural Engineering 144 (4) (2018) 04018015.

[83] H. Talebiyan, L. Dueñas-Osorio, Decentralized Decision Making for the Restoration of Interdependent Networks, ASCE-ASME Journal of Risk and Uncertainty in Engineering Systems, Part A: Civil Engineering 6 (2) (2020) 04020012.

[84] C. Johansen, I. Tien, Probabilistic multi-scale modeling of interdependencies between critical infrastructure systems for resilience, Sustainable and Resilient Infrastructure 3 (1) (2017) 1–15.
URL http://doi.org/10.1080/23789689.2017.1345253

[85] Y. Zhang, N. Yang, U. Lall, Modeling and simulation of the vulnerability of interdependent power-water infrastructure networks to cascading failures, Journal of Systems Science and Systems Engineering 25 (1) (2016) 102–118.

[86] A. Yazdani, P. Jeffrey, Complex network analysis of water distribution systems, Chaos: An Interdisciplinary Journal of Nonlinear Science 21 (1) (2011) 016111.
URL https://doi.org/10.1063/1.3540339

[87] R. Agarwal, O. Ergun, L. Houghtalen, O. O. Ozener, Optimization and Logistics Challenges in the Enterprise, Springer, 2009.
URL http://www.springerlink.com/content/u02p4653w7q3046v/

[88] D. E. Snediker, A. T. Murray, T. C. Matisziw, Decision support for network disruption mitigation, Decision Support Systems 44 (4) (2008) 954–969.

[89] W. Liu, Z. Song, Review of studies on the resilience of urban critical infrastructure networks, Reliability Engineering & System Safety 193 (June 2019) (2020) 106617.
URL https://doi.org/10.1016/j.ress.2019.106617

[90] Y. Almoghathawi, K. Barker, C. M. Rocco, C. D. Nicholson, A multi-criteria decision analysis approach for importance identification and ranking of network components, Reliability Engineering & System Safety 158 (October 2016) (2017) 142–151.
URL http://dx.doi.org/10.1016/j.ress.2016.10.007

[91] A. Beheshtian, K. P. Donaghy, R. Richard Geddes, H. Oliver Gao, Climate-adaptive planning for the long-term resilience of transportation energy infrastructure, Transportation Research Part E: Logistics and Transportation Review 113 (2018) 99–122.
URL https://doi.org/10.1016/j.tre.2018.02.009

[92] M. Wang, F. He, H. Liu, X. Lin, H. Yu, C. Li, Multi-objective optimization of distributed energy systems under uncertainty, 2020 IEEE 4th Conference on Energy Internet and Energy System Integration: Connecting the Grids Towards a Low-Carbon High-Efficiency Energy System, EI2 2020 (2020) 1670–1674.

[93] P. Seljom, L. Kvalbein, L. Hellemo, M. Kaut, M. M. Ortiz, Stochastic modelling of variable renewables in long-term energy models: Dataset, scenario generation & quality of results, Energy 236 (2021) 121415.

[94] T. Niknam, R. Azizipanah-Abarghooee, M. R. Narimani, An efficient scenario-based stochastic programming framework for multi-objective optimal micro-grid operation, Applied Energy 99 (2012) 455–470.
URL http://dx.doi.org/10.1016/j.apenergy.2012.04.017

[95] M. Kaut, Scenario generation by selection from historical data, Computational Management Science 18 (3) (2021) 411–429.
URL https://doi.org/10.1007/s10287-021-00399-4

[96] N. Löhndorf, An empirical analysis of scenario generation methods for stochastic optimization, European Journal of Operational Research 255 (1) (2016) 121–132.

[97] F. B. Abdelaziz, Solution approaches for the multiobjective stochastic programming, European Journal of Operational Research 216 (1) (2012) 1–16.
URL http://dx.doi.org/10.1016/j.ejor.2011.03.033

[98] G. Mavrotas, Effective implementation of the ϵ-constraint method in Multi-Objective Mathematical Programming problems, Applied Mathematics and Computation 213 (2) (2009) 455–465.
URL http://dx.doi.org/10.1016/j.amc.2009.03.037

[99] C. Bauckhage, NumPy / SciPy Recipes for Data Science : k -Medoids Clustering (2015).
URL https://www.researchgate.net/publication/272351873

[100] C.-l. Hwang, K. P. Yoon, Methods for Multiple Attribute Decision Making, Vol. 186, Springer-Verlag, Berlin, 1981.
URL https://doi.org/10.1007/978-3-642-48318-9_3

[101] S. Chakraborty, TOPSIS and Modified TOPSIS: A comparative analysis, Decision Analytics Journal 2 (December 2021) (2022) 100021.
URL https://doi.org/10.1016/j.dajour.2021.100021

[102] J. D. Hunter, Matplotlib: A 2D graphics environment, Computing in Science & Engineering 9 (3) (2007) 90–95.